Astronomy & Astrophysics manuscript no. lspezzi˙ChaII˙WFI˙survey˙astroph
February 9, 2007

A WFI survey in the Chamaeleon II dark cloud⋆

L. Spezzi[1], J.M. Alcalá[2], A. Frasca[1], E. Covino[2], and D. Gandolfi[3]

[1] INAF - Osservatorio Astrofisico di Catania, via S. Sofia, 78, 95123 Catania, Italy
[2] INAF - Osservatorio Astronomico di Capodimonte, Salita Moiariello, 16, 80131 Napoli, Italy
[3] Dipartimento di Fisica e Astronomia, Università di Catania, via S. Sofia 78, 95123 Catania, Italy

Received ; accepted

ABSTRACT

Aims. We present the results of an optical multi-band survey for low-mass Pre-Main Sequence (PMS) stars and young Brown Dwarfs (BDs) in the Chamaeleon II (Cha II) dark cloud. This survey constitutes the complementary optical data to the c2d Spitzer Legacy survey in Cha II.
Methods. Using the Wide-Field Imager (WFI) at the ESO 2.2 m telescope, we surveyed a sky area of about 1.75 square degrees in Cha II. The region was observed in the R_c, I_c and z broad-bands, in Hα and in two medium-band filters centered at 856 and 914 nm. We select PMS star and young BD candidates using colour-magnitude diagrams (CMDs) and theoretical isochrones reproduced *ad-hoc* for the WFI at the ESO2.2m telescope system. The selection criteria are also reinforced by using the previously known PMS stars in Cha II to define the PMS locus on the CMDs and by investigating the infrared (IR) colours of the candidates. By exploiting the WFI intermediate-band photometry we also estimate the effective temperature and the level of Hα emission of the candidates.
Results. Our survey, which is one of the largest and deepest optical surveys conducted so far in Cha II, recovered the majority of the PMS stars and 10 member candidates of the cloud from previous IR surveys. In addition, the survey revealed 10 new potential members. From our photometric characterisation, we estimate that some 50% of the 20 candidates will result in true Cha II members. Based on our temperature estimates, we conclude that several of these objects are expected to be sub-stellar and give a first estimate of the fraction of sub-stellar objects.

Key words. stars:low-mass, brown dwarfs – stars: formation – stars: pre-main sequence – ISM: clouds – ISM: individual objects: Chamaeleon II

1. Introduction

Recent investigations in star-forming regions (SFRs) have pointed out that the fraction of young Brown Dwarfs (BDs) relative to low-mass and more massive Pre-Main Sequence (PMS) stars may vary significantly among different SFRs (Kroupa 2002). In particular, the fraction is different in T and in OB associations (Briceño et al. 2002; Hillenbrand & Carpenter 2000; Luhman et al. 2000; Muench et al. 2003; Preibisch et al. 2003). Different environments may give rise to different initial conditions for star and planet formation and, hence, to differences in the observed spectrum of masses (Kroupa 2001, 2002). This may have strong consequences on the Initial Mass Function (IMF), in particular in the sub-stellar domain. It has also been proposed that BDs may form as members of small groups of objects, that may be ejected by dynamical interactions before they can grow to stellar masses (Reipurth & Clarck 2001); hence, many low-mass and sub-stellar objects might have escaped detection in surveys that concentrate sharply in the cores of SFRs. Thus, one possible reason for the differences in the fraction of young sub-stellar objects in T and OB associations can in principle be ascribed to the photometric and spatial incompleteness of the imaging surveys. Spatially complete deep imaging surveys are thus crucial in order to single out low-mass star and BD candidates to be investigated by follow-up spectroscopy. Only then, problems like mass segregation in SFRs and the low-mass end of the IMF can be addressed.

In this paper, optical wide-field imaging observations in the Chamaeleon II dark cloud (hereafter Cha II), complemented with *JHK* photometry from 2MASS (Cutri et al. 2003), are used to search for low-mass PMS stars and young BDs. Our survey covers almost 2 square degrees in the Cha II cloud.

Because of its proximity to the Sun (d≈178 pc, Whittet et al. 1997), young age (0.1-10 Myr, Hughes & Hartigan 1992) and relatively high galactic latitude (b≈−15 deg, Schwartz 1991), which decreases the effects of contamination by background stars, the Cha II dark cloud is particularly well-suited for studies of low-mass PMS stars and young BDs. It is indeed characterised by the presence of objects with Hα emission (Hartigan 1993; Hughes & Hartigan

Send offprint requests to: L. Spezzi, e-mail: lspezzi@oact.inaf.it

⋆ Based on observations carried out at the European Southern Observatory, La Silla, Chile under proposals numbers 67.C-0225 and 68.C-0311.

1992), as well as of embedded Class-I and Class-II IR sources (Larson et al. 1998; Prusti et al. 1992; Whittet et al. 1991) and X-rays sources (Alcalá et al. 2000).

Investigations in the near-IR by the DENIS survey revealed several candidate young BDs in Cha II (Vuong et al. 2001); however, a spectroscopic follow-up by Barrado y Navascuès & Jayawardhana (2004), though revealing the least massive classical T Tauri star in the cloud, failed in confirming the young BD candidates. Persi et al. (2003) performed ISOCAM observations and IR spectroscopy of several objects in the core of Cha II and found a number of sources with IR excess. Their most promising candidate, ISO-CHA II 13, was confirmed recently as the first BD in the region known to be surrounded by a disk (Alcalá et al. 2006). An optical wide-field imaging survey by López Martí et al. (2005) proposed two young BD candidates. However, that survey covered only about 10% of the cloud area.

The Cha II cloud has also been included in the Spitzer Legacy survey "From Molecular Cores to Planet Forming Disks" or c2d (Evans et al. 2003) as a test case of a cloud with moderate star formation activity. Results of the c2d survey in Cha II have been published recently by Young et al. (2005), Allers et al. (2006) and Porras et al. (2006) . The data presented in this paper constitute the optical ancillary data for the c2d survey in Cha II. As such, they are part of a multi-wavelength study of the Cha II cloud which will be presented in a forthcoming paper (Alcalá et al., in preparation).

The outline of the paper is as follows. In Sec. 2 the observations, data reduction and calibration procedures are described. In Sec. 3 we present specific tools for the analysis of the photometric data. Sec. 4 describes the criteria for the selection of PMS star and BD candidates in Cha II, using the tools developed in Sec. 3. The results of the survey and, in particular, the fraction of sub-stellar objects estimated in Cha II are discussed in Sec. 5. Our conclusions are presented in Sec. 6 and, finally, a few notes on some individual objects are presented in Appendix C.

2. Observations and data reduction

2.1. Observations

The observations were carried out in two observing runs (27-30 April 2001 and 20-23 March 2002) using the Wide Field Imaging (WFI) mosaic camera attached to the ESO 2.2m telescope at La Silla (Chile). The mosaic consists of eight 2k×4k CCDs forming a 8k×8k array with a pixel scale of 0.238″/pix; hence, a single WFI pointing covers a sky area of about 30′×30′. The Cha II dark cloud has an extention of about 2 square degrees (Hughes & Hartigan 1992). Thus, seven adjacent WFI pointings allowed us to cover about 70% of the cloud area. The distribution on the sky of the WFI pointings is shown in Fig. 1. The overlap of about 2′ between adjacent pointings allowed us to check the consistency in the photometry as well as in the astrometry.

The observations were performed in the R_C, I_C and z broad-bands, in two Hα filters, narrow ($H\alpha_7$, λ_c=658 nm and FWHM=7.4 nm) and wide ($H\alpha_{12}$, λ_c=665 nm and FWHM=12.1 nm), and in two intermediate-band filters centered at 865 and 914 nm. In order to cover the gaps between the WFI CCDs and to correct for moving objects and cosmic ray hits, for every pointing a sequence of typically five ditherings was performed in each filter. The journal of the observations is presented in Tab. 1.

Table 1. Journal of the observations. The R.A. (in hh:mm:ss) and Dec. (in dd:mm:ss) of each pointing are indicated between parenthesis. Total exposure time (T_{exp}), seeing and air mass (X) values correspond to the final staked images (see Sec. 2.2).

Field (RA,DEC)	Date (d/m/y)	Filter	T_{exp} (min)	Seeing (")	X
ChaII_1†	22/03/02	Rc/162	2×5	1.2	1.48
(13:06:18,-76:44:21)	22/03/02	Ic/Iwp	2×5	1.2	1.48
	22/03/02	z+/61	2×5	1.2	1.49
	21/03/02	Hα/7	5×4	1.0	1.54
	21/03/02	Hα/12	3×5	1.0	1.51
ChaII_2	22/03/02	Rc/162	2×5	1.2	1.55
(12:57:31,-76:44:20)	22/03/02	Ic/Iwp	2×5	1.2	1.53
	22/03/02	z+/61	2×5	1.2	1.51
	21/03/02	Hα/7	5×5	1.0	1.53
	21/03/02	Hα/12	3×5	1.0	1.56
	23/03/02	856/14	4×5	1.0	1.50
	23/03/02	914/27	5×5	1.0	1.48
ChaII_3	29/04/01	Rc/162	10×5	2.7	1.84
(13:08:13,-77:14:27)	29/04/01	Ic/Iwp	10×5	2.7	1.69
	29/04/01	z+/61	10×5	2.7	1.60
	21/03/02	Hα/7	5×5	1.2	1.64
	21/03/02	Hα/12	3×5	1.2	1.59
	23/03/02	856/14	4×5	1.2	1.51
	23/03/02	914/27	5×5	1.2	1.53
ChaII_4	22/03/02	Rc/162	2×5	1.4	1.49
(12:59:03,-77:13:58)	22/03/02	Ic/Iwp	2×5	1.4	1.50
	22/03/02	z+/61	2×5	1.4	1.50
	21/03/02	Hα/7	5×5	1.2	1.50
	21/03/02	Hα/12	3×4	1.2	1.51
	23/03/02	856/14	4×5	1.2	1.57
	24/03/02	914/27	5×5	1.2	1.54
ChaII_5	22/03/02	Rc/162	2×5	1.2	1.60
(12:49:53,-77:13:59)	22/03/02	Ic/Iwp	2×5	1.2	1.62
	22/03/02	z+/61	2×5	1.2	1.66
	21/03/02	Hα/7	5×5	1.2	1.75
	21/03/02	Hα/12	3×5	1.2	1.66
	23/03/02	856/14	4×5	1.0	1.49
	23/03/02	914/27	5×5	1.0	1.50
ChaII_6	30/04/01	Rc/162	10×6	2.0	1.67
(13:10:07,-77:45:08)	30/04/01	Ic/Iwp	10×6	2.0	1.57
	30/04/01	z+/61	10×6	2.0	1.52
	21/03/02	Hα/7	5×5	1.4	1.61
	21/03/02	Hα/12	3×5	1.4	1.66
	23/03/02	856/14	4×5	1.2	1.67
	23/03/02	914/27	5×5	1.2	1.74
ChaII_7	22/03/02	Rc/162	2×4	1.2	1.78
(13:00:28,-77:44:39)	22/03/02	Ic/Iwp	2×5	1.2	1.74
	22/03/02	z+/61	2×5	1.2	1.69
	21/03/02	Hα/7	5×5	1.0	1.52
	21/03/02	Hα/12	3×5	1.0	1.51
	23/03/02	856/14	4×5	1.0	1.58
	23/03/02	914/27	5×5	1.0	1.62

† Not observed in the 856-nm and 914-nm bands.

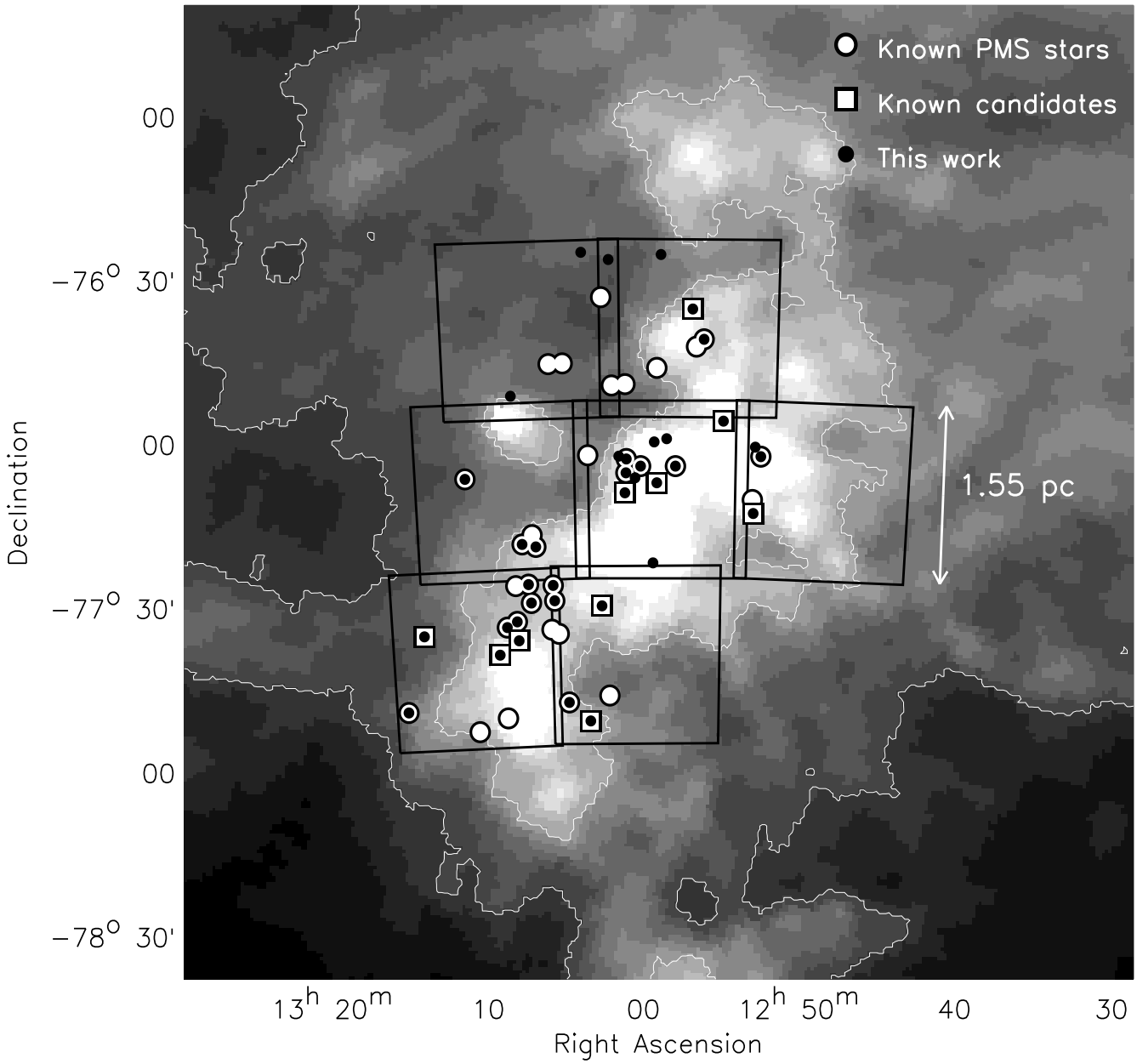

Fig. 1. IRAS 100μm dust emission map of the Cha II dark cloud. The contours, from 10 to 40 MJy $\times$ sr^{-1} in steps of 2.5 MJy $\times$ sr^{-1} are also drawn (white lines). The big polygons define the area covered by the seven ESO2.2m+WFI pointings. The confirmed members of the cloud and the candidates selected in previous surveys are represented with open circles and squares respectively; the black dots mark the objects recovered by our selection criteria (see Sec. 4). Some 13 previously known PMS stars appear saturated in at least one of the bands of our survey and this is why they appear as open circles only. However, when using photometry from the literature, these objects are also recovered from our selection criteria (see Sec. 4).

2.2. Pre-reduction and Astrometry

The pre-reduction of the raw images, passing through bias subtraction, flat-fielding and correction for fringing, was performed on a nightly basis, using the *mscred* package under IRAF[1], following the guidelines described in Alcalá et al. (2002). The resulting pre-reduced images are uniform to about 1%. In order to correct for large-scale illumination variations a super-flat was used.

The astrometric calibration and relative flux scaling between ditherings were done using the ASTROMETRIX tool[2]. ASTROMETRIX performs a global astrometric solution which takes into account overlapping sources falling on adjacent CCDs in different ditherings. For each pointing, the astrometric solution was first computed for the *R*-band dithering-set using

[1] IRAF is distributed by the National Optical Astronomy Observatories (NOAO).

[2] Available at: http://www.na.astro.it~radovich.

the USNO-A2.0 catalogue (Monet et al. 1998) as a reference. A catalogue of sources was then extracted from the re-sampled *R*-band image and used as reference catalogue for all the other bands. Within the global astrometry process, the astrometric solution was constrained for each CCD by both the positions from the *R*-band catalogue and those from overlapping sources in all the other CCDs. The co-addition of the different dithered images for a given filter and pointing was performed using the SWARP tool[3]. The resulting 8k×8k stacked images were normalised by the exposure time. The absolute astrometric precision of our images is about 0.35 arcsec, corresponding to the RMS accuracy of the USNO-A2.0 catalogue, while the internal RMS, computed from overlapping sources in different exposures, is within 0.05 arcsec, indicating the good performance of ASTROMETRIX.

2.3. The photometric calibration

In order to transform the *R* and *I* instrumental magnitudes to the standard Cousins system, the Landolt standard fields SA 98, SA 101 and SA 107 (Landolt 1992) were observed nightly. The standard R_C and I_C magnitudes were determined using the transformation equations:

$$R_C = r_0 + c_R \cdot (r_0 - i_0) + ZP_R \quad (1)$$

$$I_C = i_0 + c_I \cdot (r_0 - i_0) + ZP_I \quad (2)$$

where r_0 and i_0 are the instrumental magnitudes corrected for atmospheric extinction and c_R and ZP_R and c_I and ZP_I the colour terms and zero points for the *R* and *I* bands respectively. The standard magnitudes from Stetson (2000) were used in order to determine the zero points and colour terms.

The intermediate-band instrumental photometry was transformed to the standard AB photometric system following the prescriptions by Jacoby et al. (1987) and Alcalá et al. (2002) by using the equation:

$$m_{AB}(\lambda) = m_0(\lambda) + ZP_\lambda \quad (3)$$

where m_0 is the instrumental magnitude in a given intermediate-band filter corrected for atmospheric extinction and ZP_λ the zero point derived by using the spectrophotometric standard stars Hiltner 600, LTT 4364 and Eg 274 (Hamuy et al. 1992), observed by us in the same run. The resulting magnitudes in the intermediate band filters are in the AB system.

The nightly calibration coefficients are reported in Tab. 2.

2.3.1. The *z*-band photometric calibration

The calibration of the *z* magnitudes required more effort as there are no data for standard stars available in the literature. Since we aimed at determining the colour-magnitude diagrams (CMDs) of the sources in Cha II (Sec. 4) and their spectral energy distributions (SEDs, Sec. 5), we needed both to tie the *z* magnitudes with some "reference" photometric system and to determine the flux at Earth of a star with magnitude $z = 0$. To this aim, we observed the same Landolt standard fields in the *z* filter. In the Landolt SA 98 field we selected the A0-type star SA 98 653, whose visual magnitude and colours are reported in Tab. 3. This star is very well characterised and its absolute spectrophotometry is well determined (Gutièrrez Moreno et al. 1988). For this A0-type star we can assume $(I_C - z) = 0$, thus defining the "standard" *z*-magnitude system as that for which the colour $(I_C - z)$ is zero for A0 type stars. The zero point of this calibration is then determined as follows:

$$Zp = z - z_0 = I_C - z_0 \quad (4)$$

where $I_C = 9.522$ is the standard magnitude of SA 98 653 in the Cousins system and z_0 its *z*-band instrumental magnitude corrected for atmospheric extinction. We then applied this zero point correction to the z_0 instrumental magnitude of all the stars in the Landolt fields. In this way we obtained a catalogue of Landolt stars with *z* magnitudes and $(I - z)$ colours in our internal WFI-Cousins system. We then used this catalogue to find the least squares solution to the equation:

$$z = z_0 + c_z \cdot (i_0 - z_0) + ZP_z \quad (5)$$

where z_0 and i_0 are the standard stars instrumental magnitudes corrected for atmospheric extinction and ZP_z and c_z the *z* calibration coefficients for the newly defined WFI-Cousins photometric system. The nightly mean values obtained for ZP_z and c_z are reported in Tab. 2.

Since the absolute spectrophotometry of SA 98 653 is available from Gutièrrez Moreno et al. (1988), we can use this star

Table 2. Photometric calibration coefficients (atmospheric extinction coefficient, *K*, zero point, *ZP*, and colour terms, *c*) for the WFI filters used in this work.

Filter	Date	$K^\dagger$	*ZP*	*c*
R	04/27/2001	0.096	24.418±0.004	-0.038±0.010
”	04/28/2001	0.096	24.388±0.001	-0.056±0.008
”	04/29/2001	0.096	24.445±0.004	-0.023±0.003
”	03/21/2002	0.096	24.397±0.003	-0.030±0.003
I	04/27/2001	0.082	23.413±0.012	0.222±0.002
”	04/28/2001	0.082	23.399±0.001	0.216±0.003
”	04/29/2001	0.082	23.431±0.001	0.221±0.007
”	03/21/2002	0.082	23.335±0.001	0.222±0.002
z	04/27/2001	0.080	21.546±0.804	0.336±0.311
”	04/28/2001	0.080	21.246±0.303	0.230±0.143
”	04/29/2001	0.080	21.248±0.353	0.214±0.140
”	03/21/2002	0.080	21.460±0.014	0.373±0.001
$H\alpha_7$	03/20/2002	0.096	21.249±0.095	/
$H\alpha_{12}$	03/20/2002	0.096	21.733±0.133	/
856*nm*	03/22/2002	0.080	20.894±0.089	/
914*nm*	03/22/2002	0.080	21.018±0.082	/

† The mean atmospheric extinction coefficients for La Silla have been adopted.

[3] Available at: http://terapix.iap.fr/cplt/oldSite/soft/swarp.

Table 3. Standard photometry of SA 98 653 (R.A. = 06:52:05, Dec. = −00:18:18) from Stetson (2000).

V	$(B-V)$	$(U-B)$	$(V-R_C)$	$(R-I)_C$
9.539	−0.004	−0.097	0.007	0.008

to obtain the absolute flux calibration in the z filter, i.e. to obtain the flux at Earth of a star with z=0. Following the procedure outlined in Appendix A we derive:

$$F(z=0) = (8.4 \pm 0.1) \cdot 10^{-10} \ \text{erg cm}^{-2}\ \text{s}^{-1}\ \text{Å}^{-1}$$

$$= (2608 \pm 31)\ \text{Jy}$$

This value can be used to derive the flux in the z-band of the sources in our catalogue using their corresponding z-band magnitudes.

2.4. The catalogue extraction

2.4.1. PSF fitting procedure

PSF fitting photometry has been performed by using the IRAF/daophot package (Stetson 1987). Since we are interested in the faintest stellar objects, the threshold level was defined in order to select all the sources having a signal-to-noise ratio (σ) greater than 3. This choice may lead to the extraction of many spurious detections, however *daophot* allows us to discriminate between stars, extended sources (galaxies), saturated objects and other spurious detections. The PSF fitting procedure was re-iterated twice for each Cha II field; given the moderate crowding of these fields, this choice allowed us to detect the faintest neighbours to bright stars while keeping the number of spurious detections relatively small. The typical residual of the PSF fitting is less than 2% of the peak brightness. A single catalogue comprising all the stellar sources detected in all the available photometric bands was finally produced. In Fig. 2 the internal photometric errors of all the detected point-like sources are plotted against the magnitude for all the available filters; the relative exponential fits are over-plotted. Tab. 4 summarises the number of point-like sources detected in the surveyed area in each filter and the limiting magnitudes achieved at the 10σ, 5σ and 3σ levels, respectively.

2.4.2. Completeness

The completeness of our catalogues was estimated in the standard way by inserting artificial stars into the images and recovering them using the same extraction parameters as for the real objects; the fraction of the recovered artificial objects provides a measure of the completeness. We used the IRAF/addstar package to perform the exercise. We inserted 3000 artificial sources; this number should not alter significantly the crowding statistics in the images. The profile for the artificial sources was

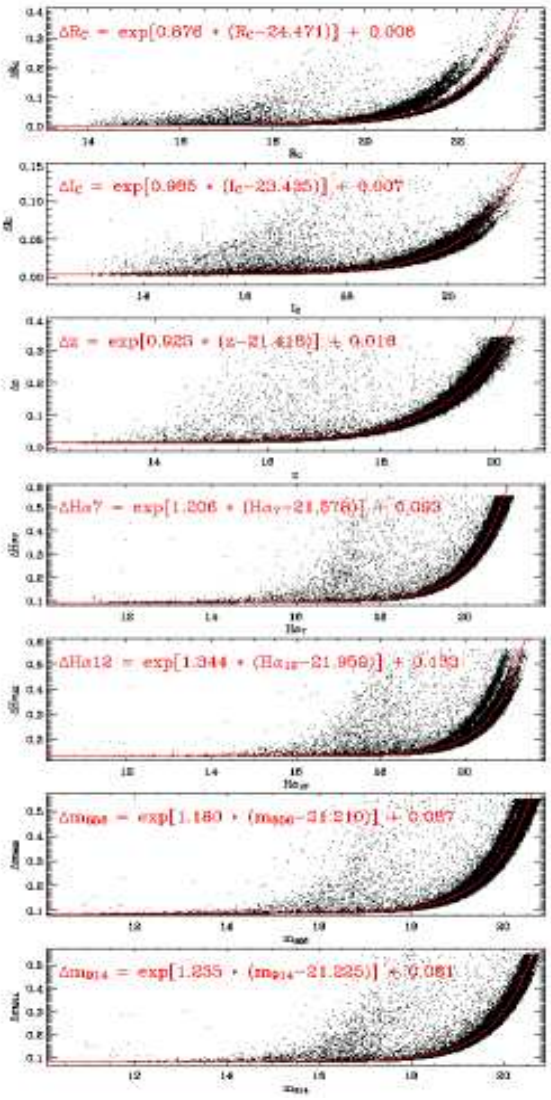

Fig. 2. Photometric errors versus magnitudes and relative exponential fits for all the point-like sources detected in Cha II and for all the available filters. The "double sequence", clearly visible in R and $H\alpha_{12}$ bands, is due to different seeing conditions in the individual exposures.

generated by using the same PSF model used for the source extraction; the position of the artificial objects are randomly distributed over the entire area of the mosaic and their magnitudes range uniformly between the detection and the saturation limits in each band. As an example we show the results for the ChaII_2 field (see Tab. 1). Fig. 3 shows the fraction of recovered artificial objects as a function of magnitude for each filter. The corresponding magnitude limits at 95% completeness level (C=95%) are reported in Tab. 4.

3. Tools for candidates selection

Our primary criterion for the selection of low-mass PMS star and BD candidates from the extracted catalogue was based on the comparison of the object location in CMDs with theoretical isochrones. In addition, our WFI data in the 865-nm and 914-

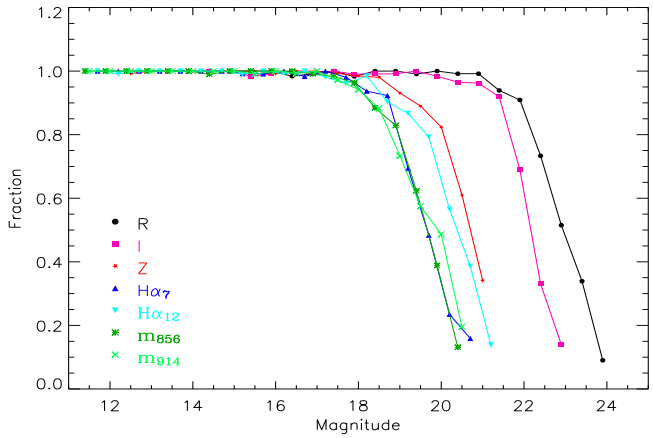

Fig. 3. Completeness plots for extraction of artificial stars from the ChaII_2 mosaic (see Tab. 1) for all the photometric bands used in this work (see text).

Table 4. Number of stellar sources (N*) detected in each filter and relative limiting magnitudes at the 10σ, 5σ and 3σ level. The last column report the magnitude limit at 95% completeness level.

Filter	N*	Mag 10σ	Mag 5σ	Mag 3σ	Mag (C=95%)
Rc/162	141400	21.8	22.6	23.2	21.3
Ic/Iwp	141000	21.0	21.7	22.3	21.0
z+/61	79000	18.7	19.6	20.2	18.8
Hα/7	72500	17.5	19.8	20.4	18.0
Hα/12	84200	17.8	19.9	20.8	18.4
856-nm	76700	18.6	19.4	20.0	18.0
914-nm	80400	18.9	19.5	20.1	18.0

nm intermediate-bands allowed us to obtain a first estimate on the effective temperature of the candidates, whereas the measurements in Hα provided us with a diagnostics for possible Hα emission. Our selection method exploits the tools which are now described.

3.1. Theoretical Isochrones

Theoretical isochrones for low-mass stars and BDs down to 0.001 $M_\odot$ are provided by Baraffe et al. (1998) and Chabrier et al. (2000) in the Cousins photometric system (Bessel 1990). Since the WFI filters transmission curves are somewhat different from the original Cousins ones, in particular for the *I*-band, it is crucial to transform the colours and magnitudes into the appropriate photometric system. We thus transformed the isochrones by Baraffe et al. (1998) and Chabrier et al. (2000) into the WFI-Cousins system as described in Appendix B. In this way, we can use the isochrones to define the PMS locus in the CMDs (e.g. Fig. 9) in a photometrically consistent way.

In Fig. 4 the theoretical R_C vs. $(R\text{-}I)_C$ colour-magnitude diagram is shown. The 95% completeness limit was determined from the values reported in Tab. 4. For A_V=0 we are complete down to 0.02 $M_\odot$ at the 95% level for objects younger than 10 Myr. For an average extinction $A_V \approx$2 mag for Cha II (Cambrésy 1999) a 95% completeness limit corresponds to 0.03 $M_\odot$.

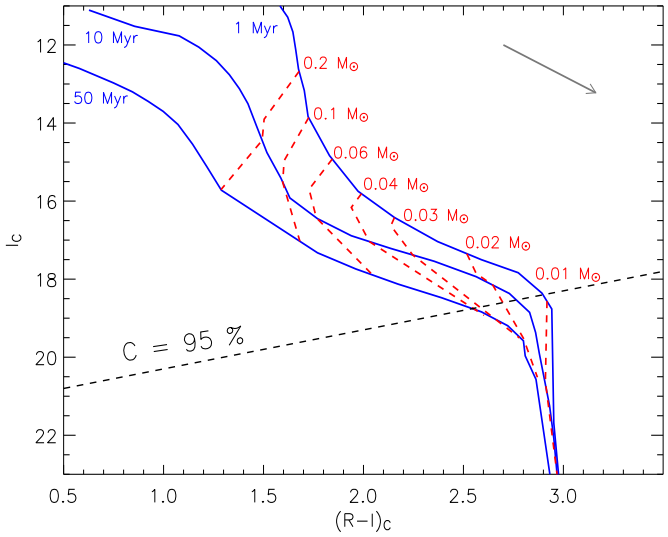

Fig. 4. Theoretical R_C vs. $(R\text{-}I)_C$ diagram. The isochrones (continuous curves) and PMS tracks (dashed curves), shifted to the distance modulus of Cha II (6.25 mag, Whittet et al. (1997)) are in the WFI-Cousins photometric system. The dashed straight line represents the 95% completeness limit. The A_V=2 mag reddening vector is shown.

3.2. The ($m_{856} - m_{914}$) index vs. temperature relation

Late-type dwarfs are characterised by strong molecular absorption bands essentially due to metallic oxides (TiO and VO). The ESO-WFI medium-band filter centered at 856 nm covers important TiO absorption features that deepen with decreasing temperature, while the medium-band filter centered at 914 nm lies in a wavelength range which is relatively featureless in late-type objects (see Fig. B.1 lower panel in Appendix B). Thus, the ($m_{856} - m_{914}$) colour index is sensitive to the effective temperature for very cool objects (2000 K$\lesssim T_{eff} \lesssim$3800 K), where TiO dominates the opacity (Allard 1990; Burrows & Liebert 1993; O'Neal et al. 1998). In the absence of interstellar extinction, this index can provide a first reliable guess of the temperature of the cool candidates.

Using the filter transmission curves for the corresponding intermediate-band filters and the synthetic low-resolution StarDusty spectra for low-mass stars and BDs by Allard et al. (2000) we derived the relationship between the ($m_{856} - m_{914}$) index and the effective temperature, applying the methods described in Appendix B. The synthetic ($m_{856} - m_{914}$) index, derived by integrating the StarDusty spectra under the filter transmissions and CCD quantum efficiency curves, is in the instrumental WFI system. As such, it was transformed into the standard AB photometric system by applying the zero points derived from the spectrophotometric standard stars Hiltner 600, LTT 4364 and Eg 274, observed with WFI in the 856-nm and 914-nm bands (see Sec. 2.3). From the standard fluxes (Hamuy et al. 1992) integrated under the WFI passbands like-

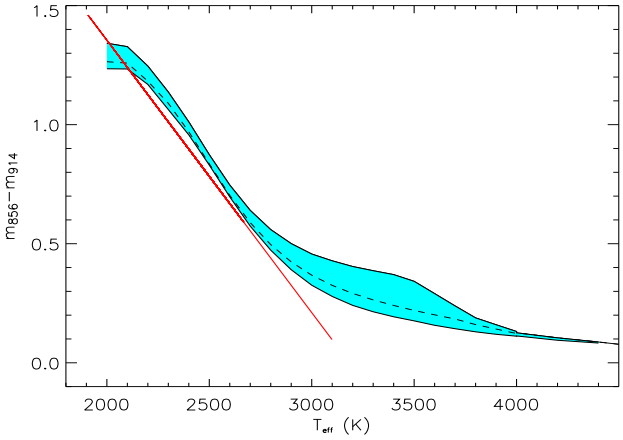

Fig. 5. ($m_{856} - m_{914}$) index versus effective temperature relation derived from the corresponding WFI intermediate-band filters and the synthetic low-resolution StarDusty spectra for low-mass stars and BDs by Allard et al. (2000). The two solid curves show the relation for $\log g$=5.0 (lower boundary) and $\log g$=3.5 (upper boundary); the dashed curve represents the T_{eff}-colour relation for $\log g$=4.0. The straight line is the empirical relationship derived by López Martí et al. (2004).

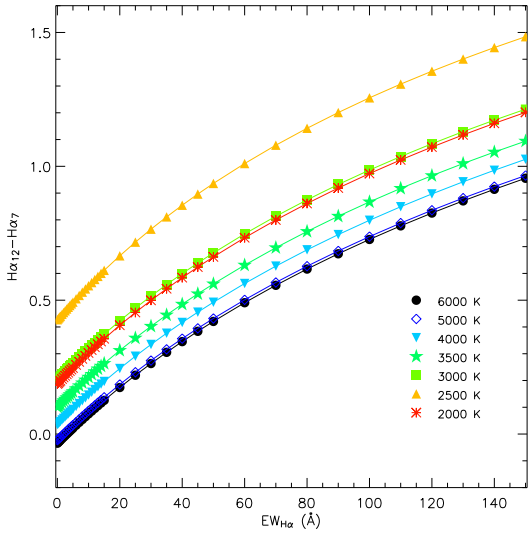

Fig. 6. Calibration relation between the ($H\alpha_{12} - H\alpha_7$) index and the Hα equivalent width derived from the corresponding WFI intermediate-band filters and the synthetic low-resolution StarDusty spectra for low-mass stars and BDs by Allard et al. (2000).

wise the StarDusty spectra, we found an average zero-point correction for the ($m_{856} - m_{914}$) colour of −0.13 mag, which allowed us to obtain the calibrated synthetic ($m_{856} - m_{914}$) index as:

$$(m_{856} - m_{914})^{synt}_{calib} = (m_{856} - m_{914})^{synt}_{instr} - 0.13 \qquad (6)$$

In Fig. 5 we show the resulting ($m_{856} - m_{914}$) index versus temperature relation. This relation depends on the stellar gravity, as indicated by the shaded area in Fig. 5, which encompasses all the calibrations for models in the range 3.5≤ $\log g$ ≤5. We also derived this relationship using other stellar atmosphere models (e.g. NextGen, COND, etc.); the StarDusty models were chosen because they better match the empirical relationship between the ($m_{856} - m_{914}$) index and the effective temperature by López Martí et al. (2004) (straight line in Fig. 5). Furthermore, Allard et al. (2001) found that silicate dust grains can form abundantly in the outer atmospheric layers of the latest M dwarfs and BDs.

In the case of high interstellar extinction ($A_V \gtrsim$4 mag), the temperature derived from this relation may be underestimated because the ($m_{856} - m_{914}$) index becomes larger than in the absence of extinction. Thus, without any reliable evaluation of A_V, we can use these temperature estimates only for candidate selection purposes (see Sec. 4).

3.3. Hα Equivalent Width calibration

The WFI $H\alpha_7$ filter covers the Hα line, while the $H\alpha_{12}$ filter lies in a wavelength range which is affected by neither the Hα wings nor strong photospheric lines (see Fig. B.1 mid panel in Appendix B). The ($Ha_{12} - Ha_7$) index is thus sensitive to the intensity of the Hα line. We used the StarDusty spectra by Allard et al. (2000) to define a calibration relation between this index and the Hα equivalent width ($EW_{H\alpha}$). In order to simulate stellar spectra with different values of $EW_{H\alpha}$, we added to the synthetic spectra a Gaussian emission profile centered at Hα (656.2 nm) and having a FWHM of 3 Å. The latter value was fixed by considering the Hα line profiles of a sample of 75 PMS stars presented by Fernàndez et al. (1995); we found that the typical FWHM of the Hα emission lines of these objects is around 3 Å, though it can be higher for classical T Tauri stars (5-6 Å). However, from tests made by using profiles with different FWHM, we have verified that the FWHM value has no significant effect on the ($H\alpha_{12} - H\alpha_7$) vs. $EW_{H\alpha}$ calibration.

By applying the method described in Appendix B and correcting the synthetic ($H\alpha_{12} - H\alpha_7$) colour by the mean ($H\alpha_{12} - H\alpha_7$) colour of the spectrophotometric standard stars used to transform the intermediate-band photometry into the AB system (see Sec. 2.3), we obtained the calibration relation ($H\alpha_{12} - H\alpha_7$) vs. $EW_{H\alpha}$ displayed in Fig. 6. This relation does not depend on the FWHM of the Gaussian emission core but is strongly dependent on the effective temperature for objects cooler than about 4500 K. As expected from the contribution of the Hα absorption wings (see Fig. B.1, mid panel), for a fixed $EW_{H\alpha}$ the ($H\alpha_{12} - H\alpha_7$) index is higher for cooler objects; between 3000 and 2000 K this trend is inverted because the $H\alpha_{12}$ filter covers strong molecular absoption bands that heavily affect the continuum of very cool stars.

The relationship between the Hα index and $EW_{H\alpha}$ derived above was checked by using unpublished WFI Hα photometry and spectroscopy of already confirmed PMS stars in the L1616 cometary cloud obtained with HYDRA@WIYN3.5m (Alcalá et al. 2004) and FORS@VLT (Alcalá et al., in preparation). The spectra of the PMS stars in L1616 were integrated under the transmission curves of the WFI Hα filters to derive their "synthetic" ($H\alpha_{12} - H\alpha_7$) index. Such index was then transformed into the AB system by using the mean Hα colour

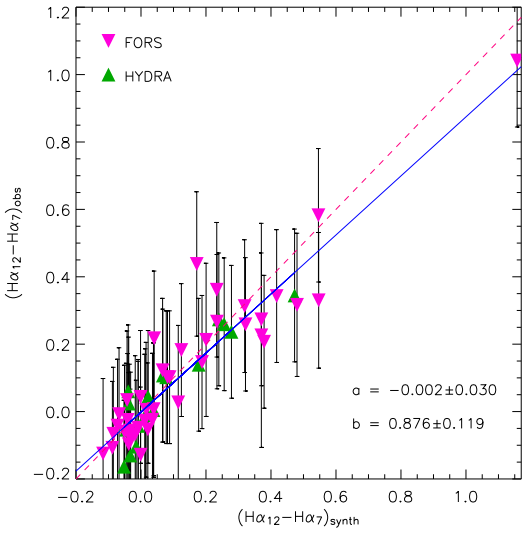

Fig. 7. ($H\alpha_{12} - H\alpha_7$) observed colours for PMS stars in L1616 as a function of the synthetic ($H\alpha_{12} - H\alpha_7$) colours (see text). The continuous line represents the best fit of the data; the dashed line has offset a=0 and slope b=1.

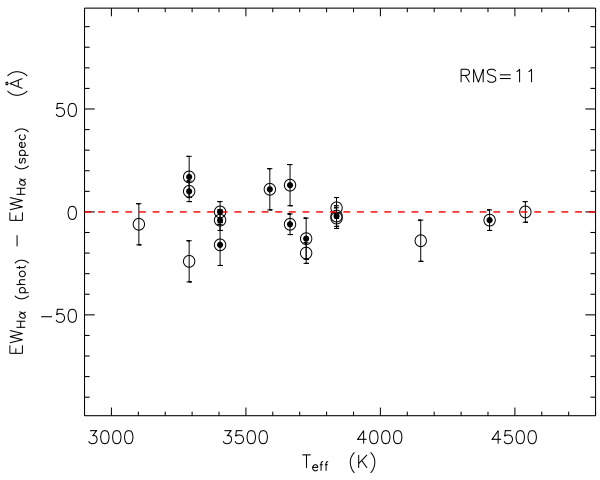

Fig. 8. Comparison between the Hα equivalent width estimated in this work from the ($H\alpha_{12} - H\alpha_7$) photometric index and that measured by Hughes & Hartigan (1992) and Barrado y Navascuès & Jayawardhana (2004) for confirmed PMS stars in Cha II (open circles). The smaller black dots mark the objects recovered by our selection criteria (see Sec. 4).

index of the corresponding spectrophotometric standard stars observed in the L1616 run. The WFI Hα photometry of these PMS stars was then used to compare the observed ($H\alpha_{12}-H\alpha_7$) index with the one derived from the spectra. Fig. 7 shows the results. The best fitting line (continuous line in Fig. 7) has a slope close to 1 and an offset close to zero; this implies that no significant correction must be applied to the ($H\alpha_{12} - H\alpha_7$) vs. $EW_{H\alpha}$ relation deduced from the synthetic spectra. Based on the errors of the observed ($H\alpha_{12} - H\alpha_7$) index we conclude that *bona-fide* emission line objects will have an Hα index greater than 0.1, corresponding to $EW_{H\alpha} \approx 10$ Å for an object with $T_{eff} \approx 4000$ K.

The Hα index versus $EW_{H\alpha}$ relation was also checked using data from the literature for the Cha II PMS stars. In Fig. 8 the Hα equivalent width derived from spectroscopic data (Hughes & Hartigan 1992), $EW_{H\alpha}$ (spec), is compared with the one derived from the Hα photometric index, $EW_{H\alpha}$ (phot). In order to estimate the latter, the effective temperatures reported by Hughes & Hartigan (1992) were used, while for the PMS star C 41 the temperature reported by Barrado y Navascuès & Jayawardhana (2004) was used. From Fig. 8, the $EW_{H\alpha}$ values derived from the Hα photometric index are in good agreement with those derived from spectroscopic data. The computed RMS suggests that the relationship shown in Fig. 6 can be used to estimate the $EW_{H\alpha}$ from the WFI Hα photometry for objects with $EW_{H\alpha} \gtrsim 10$ Å and $EW_{H\alpha} \gtrsim 30$ Å, at the 1σ and 3σ levels respectively, provided we have an estimate of the stellar temperature.

4. Selection of the candidates

For the selection of low-mass PMS star and young BD candidates we exploited both the optical data from our survey and the *JHK* photometry available from the 2MASS catalogue (Cutri et al. 2003), using the tools described in the previous sections. A matching radius of 0.5″was used to merge the WFI and the 2MASS catalogues; this value was set by taking into account the astrometric accuracy of both catalogues.

Low-mass PMS star and BD candidates in SFRs can be identified in optical CMDs. In such diagrams the colour increases rapidly for late spectral types and hence, the contamination from foreground stars is expected to decrease.

A first sample of candidates was then selected based on the I_C vs. ($I_C - z$) and I_C vs. $(R - I)_C$ CMDs. All the point-like sources detected in Cha II above the 3σ level were placed in these CMDs (Fig. 9) and their position was compared with the theoretical isochrones. The isochrones transformed into the WFI-Cousins system, as described in Sec. 3.1, were scaled to the Cha II distance of 178 pc (Whittet et al. 1997) in both CMDs. We then selected all the objects falling above the 10 Myr isochrone in both CMDs (Fig. 9). This criterion takes into account the age spread of the previously known PMS stars in Cha II (0.1-10 Myr, Hughes & Hartigan 1992) and the PMS locus that they define on the CMDs, as well as the uncertainties in interstellar extinction. In this way we selected 114 objects of which 17 were previously known Cha II members.

However, the 97 new candidates from the selection above may still be contaminated by background giants and highly-reddened objects. We therefore investigated the properties of the selected sample in the *JHK* bands using their 2MASS magnitudes. It has been found by different authors that the intrinsic ($J - H$) and ($H - K$) colours of young late-M objects are dwarf-like with, in some cases, an ($H - K$) excess, mainly arising from a circumstellar disk or an in-falling envelope (Lee et al. 2005; Luhman & Rieke 1999; Meyer et al. 1997). Furthermore, Meyer et al. (1997) found that classical T Tauri stars, with prominent IR excesses due to circumstellar accretion disks, exhibit a narrow range of colours in the

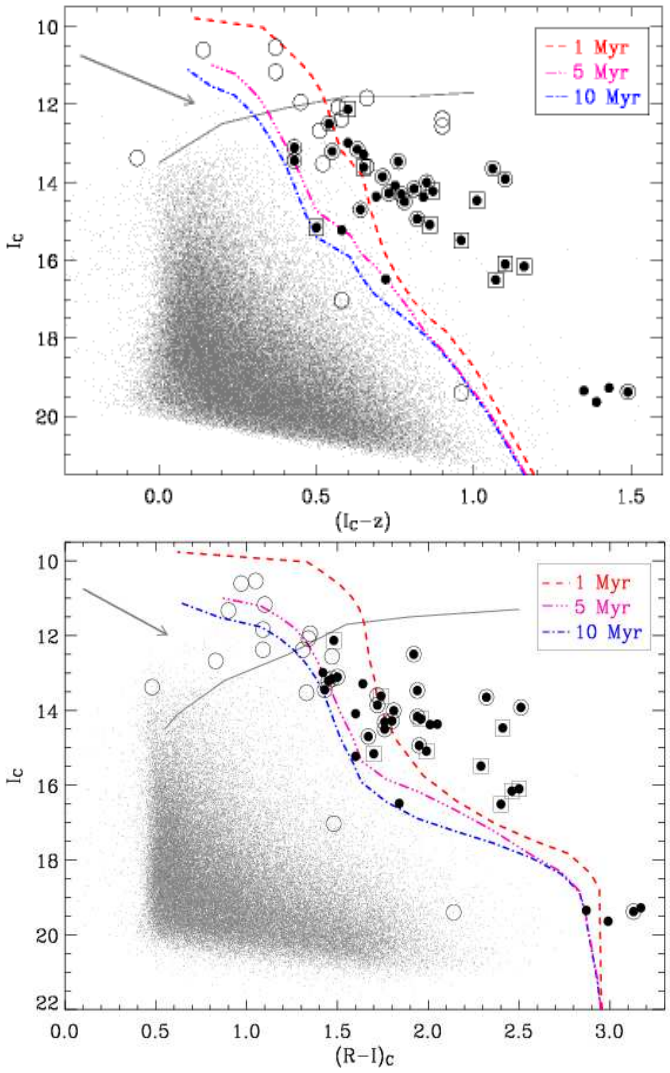

Fig. 9. I_C vs. $(I_C - z)$ and I_C vs. $(R - I)_C$ diagrams for the point-like objects in our survey (small gray dots). The lines represent the theoretical isochrones derived as explained in Sec. 3.1, shifted to the distance modulus of Cha II (6.25 mag, Whittet et al. (1997)). The continuous line in each diagram represents the saturation limit. The big black dots represent the 37 sources selected from our criteria, while the open circles and squares represent the known PMS stars and candidates selected from previous surveys respectively. The magnitudes reported by Hughes & Hartigan (1992) were used to plot the objects above and/or close to our saturation limits in any of the three broad-bands. Note that basically all the known PMS stars and candidates are recovered in our selection. The A_V=2 mag reddening vector is shown in both diagrams.

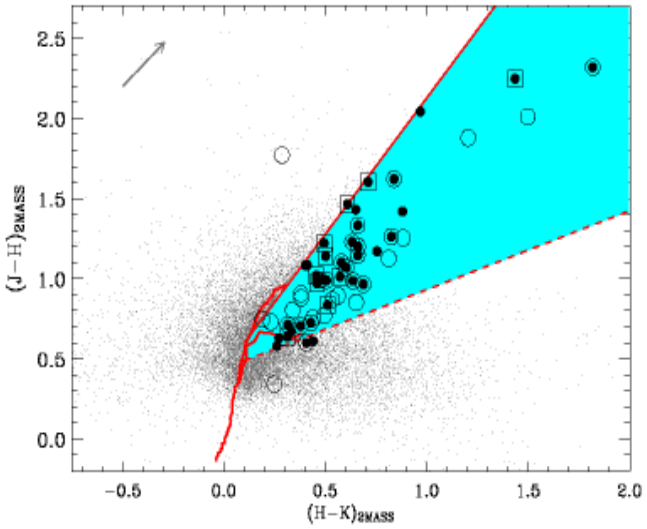

Fig. 10. $(J - H)$ vs. $(H - K)$ diagram for the sources detected in Cha II (small gray dots). The solid curve shows the relation between these indexes for main sequence stars (lower branch) and giants (upper branch). The dashed line indicates the classical T Tauri stars locus by Meyer et al. (1997). The continuous line is dividing line between giants and dwarfs. The shaded area indicates the locus presumably uncontaminated by giants. The previously known PMS stars and candidates are indicated with open circles and squares respectively. The big black dots represent the objects selected in this work. The A_V=2 mag reddening vector is shown. The two PMS stars which fall outside the selection area are the heavily veiled star Sz 47 (below the shaded area) and the binary Sz 60E (above the shaded area).

$(J - H)$ vs. $(H - K)$ diagram (dashed line in Fig. 10). By using the $(J-H)$ vs. $(H-K)$ diagram we then performed a secondary selection on the sample coming from the optical CMDs, following similar criteria as in Lee et al. (2005). The sub-sample of all the objects falling below the dividing line between giants and dwarfs (c.f. Fig. 10) should be less contaminated by background giant stars. In this way we end up with a sub-sample of 84 objects, which still include the 17 previously known members.

The sub-sample passing the secondary selection may still contain foreground and highly-reddened background objects. We thus performed a third-level selection as follows. We assumed that the objects passing the primary and secondary selections above are all at the distance of Cha II and estimated their temperature and luminosity as described in Sec. 5. Although these are first guesses of the actual stellar temperatures and luminosities, these values already provide good estimates for candidate selection purposes. We then constructed the HR diagram of our candidates sample and selected all the objects falling between the birth-line and the 20 Myr isochrone, using the models by Baraffe et al. (1998) and Chabrier et al. (2000). Although the age distribution of the confirmed members of Cha II ranges between 0.1 and 10 Myr (Hughes & Hartigan 1992), the more relaxed criterion of a 20 Myr cut-off for the candidates with a high membership probability was set by taking into account the uncertainties on the distance to the Cha II cloud (Δd=18 pc, Whittet et al. 1997) and the interstellar extinction. The evolutionary tracks of low-mass PMS stars run almost parallel to the luminosity axis of the H-R diagram. Thus, though mass estimates are not greatly affected by interstellar extinction, the age dispersion may be considerably increased if the adopted extinction for each candidate is

not well determined. The mean uncertainty on our visual extinction determinations is ∼1.5 mag (see Sec. 5.3.1); this would correspond to a luminosity uncertainty of ∼16% and, hence, and age uncertainty of ∼2 Myr for an object with mass ∼0.5$M_\odot$ and age 2-3 Myr, i.e. the typical values in Cha II (Alcalá et al., in preparation). Thus, the criterion of the 20 Myr isochrone ensures that the selected objects are, to a first approximation, consistent with Cha II membership.

The theoretical isochrones depend on the physics involved in the models. As such they may be rather uncertain, in particular in the very low-mass domain. We have thus tested the reliability of our selection criteria using as test-bench the publicly available samples of confirmed PMS stars and BDs in Taurus and IC348 reported by Briceño et al. (2002) and Luhman et al. (2003), respectively. As can be seen in Fig. 14 (available only in electronic form), the selection criteria recover the vast majority of the previously known PMS stars and BDs in these regions, providing a good check that they work well on selecting these type of objects.

5. Results of the survey

The already confirmed Cha II population members consist of some 36 objects, comprised of 33 PMS stars (Alcalá et al. 2000; Hughes & Hartigan 1992; Young et al. 2005), one BD (Alcalá et al. 2006), and two planetary-mass objects (Allers et al. 2006; Jayawardhana & Ivanov 2006).

The screening of our data lead, on the other hand, to the selection of 37 interesting objects. Of these, 17 were already known (16 PMS stars plus the BD) and 10 are candidates with high probability of membership based on their selection in previous surveys (Allers et al. 2006; Persi et al. 2003; Vuong et al. 2001; Young et al. 2005). The remaining 10 selected objects are completely new candidates. The other 13 previously known PMS stars are saturated and/or close to the saturation limit in at least one of our broad-band *RIz* images and hence, we could not apply our selection criteria. However, using their magnitudes and colours from the literature (Alcalá et al. 1995; Hughes & Hartigan 1992), these objects would fall within our selection; this means that, adding these to the 17 previously known non-saturated objects, our criteria recover 30 of the 36 previously known Cha II members.

There are a few exceptions in which the above selection criteria fail: the heavily veiled T Tauri stars Sz 47 (Hughes & Hartigan 1992) and C 41 (Barrado y Navascuès & Jayawardhana 2004), which exhibit strong UV excess that affects their colours, and the Class-I source IRAS 12500-7658 (Young et al. 2005), which is a deeply embedded object. These three sources are subluminous in both CMDs. In addition, the other Class-I source, ISO-CHA II 28, is not detected in any of our images. Although this type of objects would escape our selection, they are expected to be rare in Cha II (Young et al. (2005); Alcalá et al., in preparation). The two planetary-mass candidates reported by Allers et al. (2006) also escaped selection because they were barely detected only in our I-band images. The Herbig-Haro object HH 54 (Giannini et al. 2006) and the Class-0 source BHR 86 (Garay et al. 2002) are also associated with Cha II. HH 54 was detected only in our *R*-band and Hα images, while BHR 86 was not detected in any of the optical bands. These objects will be discussed in detail in a forthcoming paper (Alcalá et al., in preparation).

In conclusion, our selection criteria recover the majority (about 80%) of the confirmed and candidate members of Cha II reported in previous surveys. For the sake of clarity, in all the diagrams we use dots to represent the 37 objects selected with our criteria, open circles to represent the already confirmed members and open squares to represent the 10 candidates selected in previous surveys. The 10 new candidates appear simply as dots in all the diagrams.

In Tab. 7 we report all the objects with at least one photometric measurement in the optical bands[4]. The table contains the confirmed members of Cha II, the candidates selected by previous surveys and the new candidates selected in this work, as well as other sources identified as possible candidates in previous studies, but which were rejected by our selection criteria. The latter sample includes objects like the candidates reported by López Martí et al. (2005)[5] and some of the sources identified by Persi et al. (2003). Comments on some individual objects are given in Appendix C.

In the following we concentrate on the sample of 20 candidates, namely the 10 candidates selected from previous surveys, but also recovered from our selection criteria, and the 10 new candidates; they are reported in Tab. 6 and their spatial distribution is shown in Fig. 1. The 10 previously known candidates we recovered in our selection have also been proposed as young members of Cha II by recent studies (Allers et al. 2006; Vuong et al. 2001; Young et al. 2005); this supports their membership to the cloud and, at the same time, the reliability of our selection method. Moreover, several of them possess Hα emission (see Sec. 5.2). We remark that these are the candidates with the highest membership likelihood but we do not exclude that a few true Cha II members could have escaped some of our selection criteria. In particular, if they are heavily veiled, deeply embedded or components of unresolved binaries. If all the 20 candidates will be confirmed by spectroscopy, the population of Cha II will increase to some 56 members. Two of the 10 new candidates in our sample (WFI J12585611-7630105 and WFI J13005531-7708295) have been spectroscopically confirmed to be PMS stars (Alcalá et al., in preparation).

5.1. Possible contaminants

One possible source of contamination of our candidates is represented by field dwarfs. In order to estimate the number of possible foreground dwarfs in the field of ChaII we followed the prescriptions by Burgasser et al. (2004). We used the low-mass luminosity function simulations from Burgasser (2004) and the absolute magnitudes for late M and L field dwarfs from

[4] Table 7 is published only in electronic form.

[5] The BD candidates selected by López Martí et al. (2005) do not comply with our selection criteria, probably because the colour effects on the isochrones due the WFI filters was not taken into account.

Dahn et al. (2002). Assuming a limiting magnitude of I=20, i.e. the I magnitude of our faintest candidates, and a mass function $dN/dM \propto M^{\alpha}$ with 0.5< α <1.5, we expect 8-10 foreground dwarfs with 2000<T_{eff} <3000 K in the ∼2 square degrees area observed in Cha II. Therefore, up to about 50% of the candidates might be foreground dwarfs unrelated to the SFR.

Another possible source of contamination is represented by faint galaxies which may have colours similar to those of PMS objects, in particular of BD candidates. From the K-band galaxy number counts toward the celestial south pole, the expected number of background galaxies with $K \lesssim$13 mag, i.e. the K magnitude of our faintest candidates, in a ∼2 square degrees area is ∼20 (Minezaki & Kobayashi 1998). For this estimate only diffuse interstellar extinction, which is negligible (∼0.02 mag) at the K-band (Jones et al. 1981), is considered. In Cha II, the extinction may be as high as $A_V \approx$6-8 mag, i.e. $A_K \approx$1 mag. Thus, in order to contaminate our sample, the background galaxies should have $K \lesssim$12 mag; the predicted galaxy number count at this magnitude is less than 2 in the surveyed area. In addition, our PSF extraction methods remove the extended objects quite efficiently; thus, the only contaminants may be eventually the point-like extra-galactic objects, mainly QSO's. According to Prescott et al. (2006) only a handful of QSO's are expected to be present in 2 square degrees for magnitudes brighter than R =20 mag. The number increases for fainter magnitudes, but the vast majority of our candidates are brighter. Thus, we do not expect that extra-galactic objects represent a major problem of contamination.

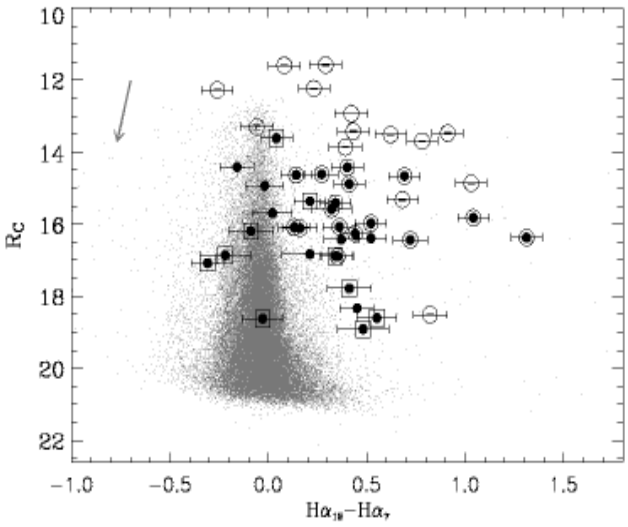

Fig. 11. R_C magnitudes versus ($H\alpha_{12} - H\alpha_7$) colours for the point-like objects in Cha II (small gray dots). The previously known PMS stars and candidates are indicated by open circles and squares respectively, whereas the sources selected in this work are represented with big black dots. The A_V=2 mag reddening vector is shown.

5.2. Hα emission of the candidates

The calibration relation between the ($H\alpha_{12} - H\alpha_7$) index and the $EW_{H\alpha}$ (see Sec. 3.3) allows us to investigate a possible Hα emission of the candidates. Based on this calibration, a threshold of ($H\alpha_{12} - H\alpha_7$)=0.1 mag would translate into an equivalenth width $EW_{H\alpha} \approx$ 10 Å at the 1σ level of detection (c.f. Sec. 3.3). Most of the previously known PMS stars and candidates have an $H\alpha$ index larger than this value (c.f. Fig. 11). 40% of the 20 candidates show Hα emission at the 1σ level, but only 2 of the 20 show it at the 3σ level. Considering that the Hα line can be strongly variable in young objects, we cannot use the index as a major diagnostic for the selection of the candidates, but only as a consistency check on their possible PMS nature. However, the 1σ level detections are yet consistent with recent spectroscopic evidence of Hα emission (Alcalá et al., in preparation). Moreover, the $EW_{H\alpha}$ range covered by our candidates (10-35 Å) is in line with that found by White & Basri (2003) for the slowly rotating, non-accreting stars and BDs in Taurus-Auriga. For the remaining candidates the ($H\alpha_{12} - H\alpha_7$) index does not indicate clear evidence for Hα emission. For three objects (WFI J12533662-7706393, WFI J12583675-7704065, and WFI J13005297-7709478) the level of Hα emission could not be estimated because they are not detected in our Hα images (the magnitude limit is ∼20.5 mag at the 3σ level). These very faint candidates are indeed of relevant importance because their optical colours resemble those of ISO-CHA II-13 (Alcalá et al. 2006). Note that also ISO-Cha II-13 was not detected on our Hα images. The Hα information drawn from our data for the selected candidates is reported in Tab. 6.

5.3. Towards the fraction of sub-stellar objects in ChaII

An interesting and important quantity in this investigation is the number of sub-stellar objects relative to the PMS stars in Cha II. In order to determine this quantity, we must single out the sub-stellar objects. According to Chabrier et al. (2000), the sub-stellar limit for 3-4 Myr objects, the approximate age of Cha II (Alcalá et al. 2000; Cieza et al. 2005; Hughes & Hartigan 1992), falls at a temperature of about 2900 K. Using the tools described in Sec. 3 and exploiting the potential of our photometric data, we attempted a first estimate of the temperature of the candidate members of Cha II and hence, a guess on the fraction of sub-stellar candidates relative to the PMS stars. We derived first the dereddened SEDs of the candidates and then provided a first estimate of their temperature.

5.3.1. Dereddened SEDs

The SEDs were derived by merging the *RIz* WFI-Cousins photometry with the 2MASS *JHK* magnitudes. The standard fluxes at each of the optical and near-IR pass-bands have been derived from the observed magnitudes using the expression $F_\lambda = F^0_\lambda \cdot 10^{-0.4 \cdot mag^{corr}_\lambda}$, where mag^{corr}_λ is the observed magnitude corrected for interstellar reddening and F^0_λ is the Earth flux of an A0-type star of magnitude $V = 0$ (Tab. 5). In order to derive the visual extinction, A_V, a SED minimization procedure was used as follows. We assume that the observed magnitude at

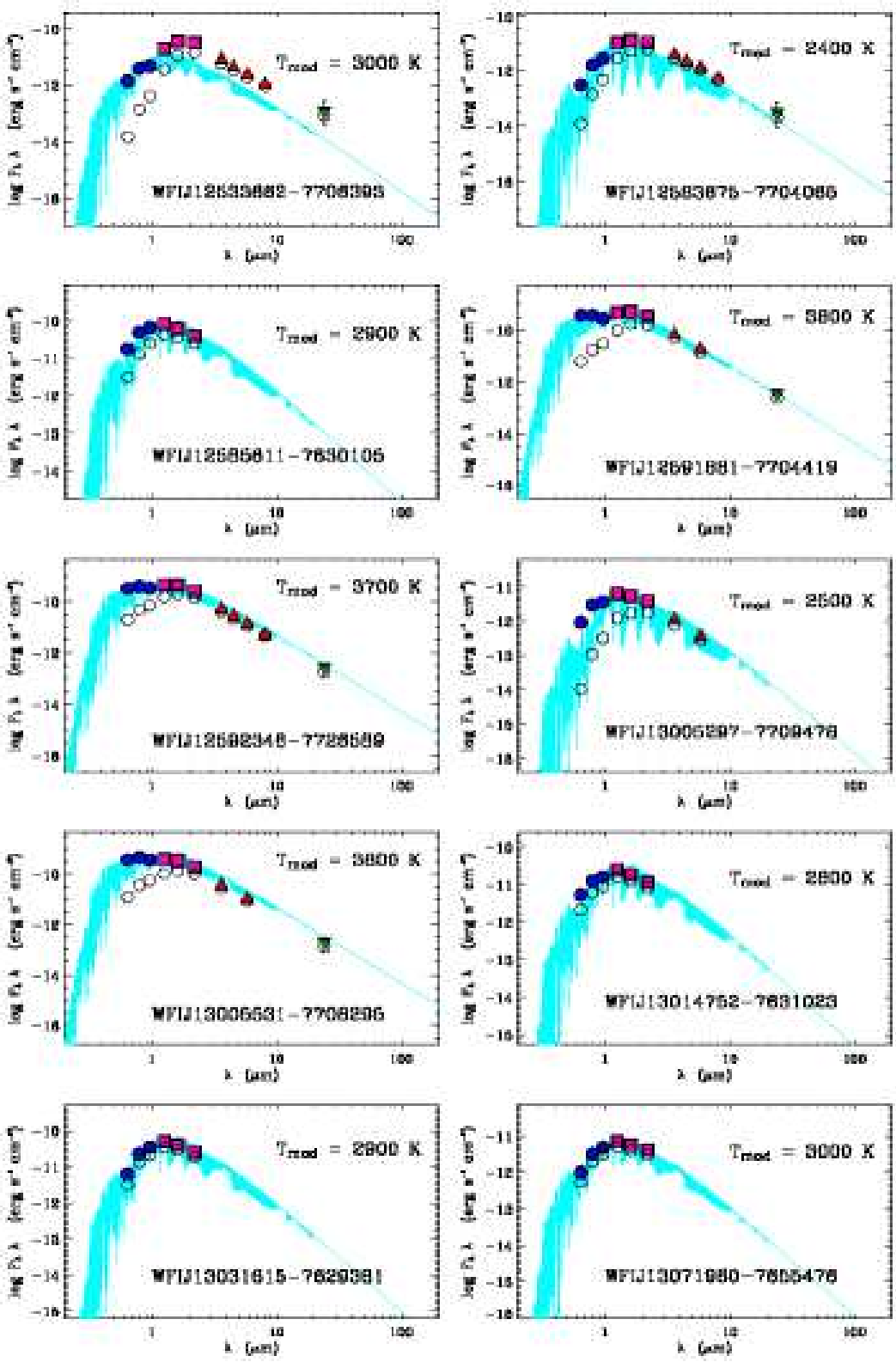

Fig. 12. Spectral energy distributions of the 10 new candidates selected in this work. Dereddened optical data are represented with filled circles; the IR data are from 2MASS (filled squares), IRAC@Spitzer and MIPS@Spitzer (filled triangles and upside down triangles respectively). The open circles represent the observed fluxes. The best fitting StarDusty spectra by Allard et al. (2000) with the same temperature as the objects are over-plotted (see Sec. 5.3.2). WFI J12585611-7630105, WFI J13014752-7631023 and WFI J13031616-7629381 fall outside the areas mapped with MIPS and IRAC; although WFI J13071960-7655476 and WFI J13005297-7709478 fall in the area surveyed with MIPS, they were not detected.

Table 5. Absolute flux calibration constants and effective wavelengths for the optical and near-IR pass-bands.

Filter	F^0_λ (erg · s^{-1} · cm^{-2} · Å^{-1})	$\lambda_{\rm eff}$ (μm)	Ref.
R_C	$2.25 \cdot 10^{-9}$	0.64	Cousins (1976)
I_C	$1.19 \cdot 10^{-9}$	0.79	Cousins (1976)
z	$8.40 \cdot 10^{-10}$	0.96	This work
J	$3.13 \cdot 10^{-10}$	1.25	Cutri et al. (2003)
H	$1.13 \cdot 10^{-10}$	1.62	Cutri et al. (2003)
K	$4.28 \cdot 10^{-11}$	2.20	Cutri et al. (2003)

each wavelength (m^λ_{obs}) can be derived by the following equation:

$$m^\lambda_{obs} - m^\lambda_{ref} = A_V \cdot \frac{dA_\lambda}{dA_V} + S \qquad (7)$$

where m^λ_{ref} is a distance-scaled reference magnitude at a given wavelength (λ) and temperature ($T_{\rm eff}$). In Eq. 7 A_V is the visual extinction, A_λ the wavelength-dependent extinction and S a scaling factor depending only on the stellar radius. Using a grid of reference magnitudes and temperatures, we perform a linear fit to the previous expression were $\frac{dA_\lambda}{dA_V}$ and $m^\lambda_{obs} - m^\lambda_{ref}$ are the independent and dependent variables, respectively, and A_V and S the two free parameters of the fit. The $\frac{dA_\lambda}{dA_V}$ term was derived using the extinction law by Cardelli et al. (1989), assuming the standard value R_V=3.1. The grid of reference SEDs was constructed by combining the tabulations of colours as function of spectral types by Kenyon & Hartmann (1995), Luhman et al. (2003) and Ducati et al. (2001). The A_V value of the reference SED minimizing the χ^2 of the fit corresponds to the best approximation of the actual visual extinction. As a check, we have compared the results from our fitting procedure with the extinction derived from the spectral types and the observed colours of previously known PMS stars in Cha II. The RMS difference in A_V is less than 1.5 mag, with only one object having a residual of about 4 mag.

In Fig. 12 the SEDs of the 10 new candidates selected in this work are shown. For six of these, we found a match in the c2d Spitzer catalogues and their IRAC and/or MIPS fluxes are also included. As appears from their SEDs, no significant IR excess is detected in these six objects. If they will be spectroscopically confirmed as Cha II members, they will most likely correspond to weak-line T Tauri stars (WTTS) or to BDs with thin disks. For the four remaining objects lacking Spitzer data we cannot assess the presence of strong IR excess. However, for three of the latter we estimate an Hα equivalenth width greater than about 20Å.

It is interesting to note that the number of WTTS relative to CTTS in Cha II is very small. Even assuming that all the candidates in our sample (see Tab. 6) would result in WTTS, which is not likely because several of them show evidence for strong Hα emission, the CTTS would outnumber the WTTS by a factor ∼2. This would be in contrast with what it is found

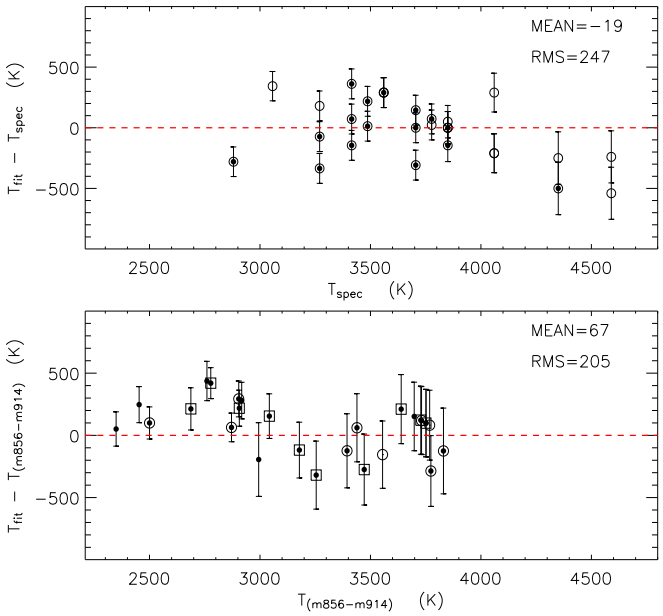

Fig. 13. Upper panel: comparison between the effective temperature resulting from the SED fitting procedure described in Sec. 5.3.2 and that derived from the spectral classification for the confirmed T Tauri stars in Cha II reported by Hughes & Hartigan (1992) and, for C 41, by Barrado y Navascuès & Jayawardhana (2004) (open circles). The black dots mark the objects recovered by our selection criteria. The point at $T_{\rm spec}$ ≈2900 K represents ISO-CHA II 13 as reported by Alcalá et al. (2006). Lower Panel: comparison between the effective temperature resulting from the SED fitting procedure described in Sec. 5.3.2 and that derived from the $T_{\rm eff}$ vs. ($m_{856} - m_{914}$) calibration. The open circles and squares represent previously known PMS stars and candidates respectively. The black dots mark the objects recovered by our selection criteria

in other clouds, like Cha I and Taurus, where WTTS dominate the PMS population (Feigelson & Montmerle 1999). Our selection based on the ($J - H$) vs. ($H - K$) diagram, picks up objects later than about K5. This might lead to the conclusion that some earlier type WTTS could have escaped our selection. However, such objects would have been detected in the previous ROSAT X-ray surveys by Alcalá et al. (1995, 2000). Only two WTTS in the cloud, namely RXJ1301.0-7654a and RXJ1303.1-7706 were discovered in such surveys. Thus, the low fraction of WTTS in Cha II seems to be real. More details on this will be discussed in a future c2d paper (Alcalá et al., in preparation), with a more complete set of SEDs for the Cha II members.

5.3.2. Temperature

The temperature of the candidates was estimated using the $T_{\rm eff}$ vs. ($m_{856} - m_{914}$) calibration relation reported in Sec. 3.2. This calibration is valid for cool objects with temperature in the range 2000–3800 K, corresponding to a dereddened ($m_{856} - m_{914}$) index in the range 1.16–0.16 mag. Thus, we ap-

plied the calibration to objects with dereddened index ($m_{856} - m_{914}$)>0.16 mag. The A_V values determined as explained in Section 5.3.1 and the extinction law by Cardelli et al. (1989) were used to deredden the ($m_{856} - m_{914}$) index. For objects with ($m_{856} - m_{914}$)<0.16 mag, i.e. hotter than about 3800 K, a temperature estimate was done by fitting a grid of reference SEDs to the dereddened SEDs. The grid of reference SEDs was constructed by combining the tabulations of colours as a function of spectral type by Kenyon & Hartmann (1995), Luhman et al. (2003) and Ducati et al. (2001); the best approximation to the dereddened SED was then obtained by χ^2-minimization of the flux differences between the dereddened SED and the reference SED. The minimization procedure was applied to the short-wavelength portion ($\lambda \leq \lambda_J$) of the SED, which is less affected by an eventual IR excess (Fig. 12). The method results to be accurate within 250 K relative to the spectroscopic temperature estimates for most of the previously known PMS stars. This is shown in the upper panel of Fig. 13, where the residuals between the temperature derived from the dereddened SED fitting, T_{fit}, and that obtained from spectroscopy by Hughes & Hartigan (1992), T_{spec}, are shown. For ISO-CHA II 13 we adopt the temperature value determined spectroscopically by Alcalá et al. (2006).

For the cool candidates, we also performed a consistency check between the temperature derived from SED fitting and that coming from the T_{eff} vs. ($m_{856} - m_{914}$) calibration. We find that the two methods yield consistent results within ~200 K, as can be seen from the lower panel of Fig. 13. We can then use the T_{eff} vs. ($m_{856} - m_{914}$) calibration confidently for those objects with dereddened ($m_{856} - m_{914}$)>0.16 mag.

The resulting temperature for each of the candidates is reported in Tab. 6. Using these estimates, we attempted to determine their radius and luminosity as follows:

1. First the reference SED of the same effective temperature as the object was selected and scaled to the Cha II distance (d= 178 pc, Whittet et al. 1997):

$$F'_{ref} = F_{ref} \cdot \left(\frac{R^\star}{d}\right)^2 \quad (8)$$

   where $R^\star$ is the stellar radius; since $R^\star$ is an unknown quantity, we let it vary between 0.1, i.e. the value expected for a BD at the Deuterium burning limit (Baraffe et al. 2003), and 10 $R_\odot$; for the objects whose effective temperature could not be estimated from the ($m_{856} - m_{914}$) index, both T_{eff} and $R^\star$ were set as free parameters in the assumption that the short-wavelength side of the dereddened SED ($\lambda \leq \lambda_J$) is mainly influenced by T_{eff};
2. the best estimate of $R^\star$ was then obtained by minimizing the flux differences between the observed dereddened SED and the reference one. The minimization procedure was performed, as above, to the short-wavelength portion ($\lambda \leq \lambda_J$) of the SED;
3. Finally, we calculated the bolometric luminosities by applying bolometric corrections to both the dereddened *I*-band and *J*-band data. Bolometric corrections were taken from Kenyon & Hartmann (1995) for objects earlier than M6 (i.e. $T_{eff} \gtrsim$3000 K), while for cooler objects we followed the prescriptions by Luhman (1999) and combined the compilations of bolometric corrections as a function of temperature by Bessel (1991), Monet et al. (1992), Tinney et al. (1993) and Leggett et al. (1996).

Having an estimate of the temperature and luminosity of the candidates, we determined their masses and ages by comparison with the set of evolutionary tracks by Baraffe et al. (1998) and Chabrier et al. (2000) on the HR diagram.

5.4. The fraction of sub-stellar objects

Previous investigations (Alcalá et al. 2000; Hughes & Hartigan 1992) showed some evidences that the mass spectrum in Cha II might be biased towards very-low mass objects. It is thus interesting to investigate what our data suggest on this matter.

Assuming that all the 20 candidates are true cloud members, we end up with 6 candidates with $T_{eff} \leq$2900 K, i.e. below the substellar limit for 5 Myr old objects. The remaining 14 objects result to be PMS star candidates (see Tab. 6). Taking into account the BD ISO-CHA II 13 and the 33 confirmed PMS stars, the resulting fraction of sub-stellar objects ($0.02M_\odot < M < 0.08M_\odot$) relative to the PMS stars ($0.08M_\odot < M < 10M_\odot$), $R_{ss} = \frac{N(0.02-0.08)}{N(0.08-10)}$, in Cha II would be ~15% (19% if we consider the two planetary-mass objects reported by Jayawardhana & Ivanov 2006). This last value would imply a peculiar mass-spectrum for the population of Cha II relative to other T associations (where R_{ss}=12-14%, Briceño et al. 2002; López Martí et al. 2004), in particular in the sub-stellar domain. If we assume that only the candidates having Hα emission are true cloud members, the R_{ss} value would drop to ~10% (15% if we consider the two planetary-mass objects reported by Jayawardhana & Ivanov 2006), i.e. more similar to that measured in other T associations and lower than that measured in OB associations (~26%, Barrado y Navascuès et al. 2001; Boulanger et al. 1998; Briceño et al. 2002; Hillenbrand & Carpenter 2000; Muench et al. 2002). If R_{ss} in Cha II is similar as in other T associations, we expect that at least 50% of the candidates reported in Tab. 6 will be genuine Cha II members.

Assuming that the 7 IRAS sources with Hα emission discussed in Appendix C are PMS stars, the fraction of substellar objects would drop to about 8% or 13% depending on whether the two planetary-mass objects are counted among the sub-stellar ones.

By comparing the position of the candidates in the HR diagram with the Baraffe et al. (1998) and Chabrier et al. (2000) evolutionary tracks, their age distribution would peak between 2 and 3 Myr, if they were genuine Cha II members. This would be fairly consistent with the average age of 3.6 Myr determined by Cieza et al. (2005) for a sample of T Tauri stars in Cha II. Taking into account the candidates, the mean mass in Cha II would be ~0.5$M_\odot$, i.e. slightly lower than the mean mass of the confirmed members alone (0.6 $M_\odot$) and comparable to the mean mass for the Cha I population (~0.45 $M_\odot$[6]).

[6] Luminosity and temperature determinations are reported by Luhman (2004) for 144 members of Cha I. We derived masses and

Table 6. The 20 candidates selected in this work. The visual extinction (A_V) and temperature (T_{eff}) of the candidates were estimated as explained in Sec. 5.3.1 and Sec. 5.3.2, respectively. Wherever possible, the extinction and temperature values were compared with other estimates from literature.

Designation	$EW_{H\alpha}$ (Å)	A_V (mag)	T_{eff} (K)	A_V^{lit} (mag)	T_{eff}^{lit} (K)	Ref.	Classification in this work
WFI J12533662-7706393	Not Det.	5.58	†3000±250				PMS star cand.
C 17	No Em.	5.95	⋆3600±200	5.1		b	PMS star cand.
C 33	No Em.	4.48	†3700±250	2.4		b	PMS star cand.
IRAS 12535-7623	No Em.	3.38	⋆3900±200	5		a	PMS star cand.
WFI J12583675-7704065	Not Det.	3.84	†2400±200				BD cand.
WFI J12585611-7630105	30	1.91	†2900±200				BD cand.
ISO-CHA II 29	No Em.	5.94	⋆3900±200	11.5		b	PMS star cand.
WFI J12591881-7704419	No Em.	4.98	⋆3800±200				PMS star cand.
WFI J12592348-7726589	No Em.	3.33	†3700±250				PMS star cand.
WFI J13005297-7709478	Not Det.	5.50	†2500±200				BD cand.
WFI J13005531-7708295	No Em.	4.13	⋆3800±200				PMS star cand.
IRAS F12571-7657	No Em.	3.95	⋆⋆>3000	8,13		b,c	PMS star cand.
WFI J13014752-7631023	No Em.	0.88	†2800±200				BD cand.
C 50	20	3.46	†3000±200	2.0		b	PMS star cand.
C 51	20	1.16	†3300±250	2.3		b	PMS star cand.
WFI J13031615-7629381	15	0.61	†2900±200				BD cand.
C 62	35	3.53	†3000±200	4.1,4	3140	b,c	PMS star cand.
WFI J13071960-7655476	25	0.50	⋆3000±200				PMS star cand.
C 66	25	3.87	†2900±200	3.7,0	2793	b,c	BD cand.
2MASS13125238-7739182	10	1.36	†3400±250			d	PMS star cand.

Notes to column 4:
† Temperature derived from the dereddened ($m_{856} - m_{914}$) colour index (Sec. 3.2).
⋆ Temperature derived from the SED fitting method described in Sec. 5.3.2.
⋆⋆ See Appendix C.

References: a) Larson et al. (1998); b) Vuong et al. (2001); c) Allers et al. (2006); d) Young et al. (2005).

6. Conclusions

The optical survey presented here is one of the deepest and more extensive conducted so far in Cha II and constitutes the optical ancillary data for the c2d Spitzer Legacy survey in this cloud.

The photometric selection based on our optical imaging data, combined with data in the near-IR from the 2MASS, allowed us to recover basically all the previously known members of the cloud, including 10 candidates from previous IR surveys, with a high membership probability. Furthermore, we provided 10 new likely member candidates that were not detected by previous surveys, thereby increasing the total number of candidates to 20. Should all these objects be spectroscopically confirmed as PMS stars and young BDs, the population of Cha II will increase to 56 members. Up to 50% of the sample may be contaminated by field dwarfs. According to our characterisation criteria of the candidates, we estimate that at least some 50% of them will result in true Cha II members and, based on our temperature estimates, several of these objects are expected to be sub-stellar. Under these assumptions, we conclude that the fraction of substellar objects relative to the PMS stars in Cha II is on the order of ∼19%, i.e. larger than that reported for other T associations like Taurus. In the most conservative hypothesis in which only the candidates showing Hα emission would result in true member of the cloud, this fraction would drop to ∼15%, i.e. comparable with that measured in other T associations.

From the completeness of our survey, both in space and flux, we conclude that the optical population of Cha II members discovered so far is nearly complete. We do not expect to find many more PMS stars based on optical observations. More clues to these issues will be addressed in a forthcoming paper by combining the optical data presented here with those from the MIPS@Spitzer and IRAC@Spitzer observations in Cha II (Alcalá et al., in preparation).

ages for these objects using the evolutionary tracks by Baraffe et al. (1998) and Chabrier et al. (2000) in a homogeneous way.

Acknowledgements. This work was partially financed by the Istituto Nazionale di Astrofisica (INAF) and the Italian Ministero

dell'Istruzione, Universitá e Ricerca (MIUR). We thank the anonymous referee for his/her constructive comments and suggestions. We also thank M. Radovich for many explanations on the use of ASTROMETRIX. We thank N. Evans, PI of the c2d Spitzer Legacy Program, and L. Cieza for many useful comments and suggestions on an earlier version of the paper. We also thank F. Coméron and E. Marilli for discussions. L. Spezzi acknowledges financial support from COFIN-MIUR-2004 (The X-Shooter spectrograph for the VLT) and PRIN-INAF-2005 (Stellar clusters: a benchmark for star formation and stellar evolution) and a grant by the Europen Southern Observatory (ESO) for a two-months stay at Garching. Support for this work, part of the Spitzer Legacy Science Program, was provided by NASA through contract 1224608 issued by the Jet Propulsion Laboratory, California Institute of Technology, under NASA contract 1407. We also thank the Lorentz Center in Leiden for hosting several meetings that contributed to this paper. This research made use of the SIMBAD database, operated at CDS (Strasbourg, France) and the data products from the Two-Micron All-Sky Survey, which is a joint project of the University of Massachusetts and the Infrared Processing and Analysis Center at California Institute of Technology, funded by NASA and the National Science Foundation.

References

Alcalá J.M., Krautter J., Schmitt J. et al. 1995, A&A Supp. Ser. 114, 109
Alcalá J.M., Covino E., Sterzik M.F. et al. 2000, A&A 355, 629
Alcalá J.M., Radovich M., Silvotti R. et al. 2002, proceedings of the SPIE 4836, 406
Alcalá J.M., Wachter S., Covino E. et al. 2004, A&A 416, 677
Alcalá J.M., Spezzi, L., Frasca, A., Covino, E., Porras, A., Merín, B., Persi, P. 2006, A&A, 453, 1
Allard F. 1990, PhD Thesis, Ruprecht Karls Univ. Heidelberg
Allard F., Hauschildt P.H. & Schwenke D. 2000, ApJ 540, 1005
Allard F., Hauschildt P.H., Alexander D.R. et al. 2001, ApJ 556, 357
Allers K.N., Kessler-Silacci J.E., Cieza L.A. & Jaffe D.T. 2006, ApJ 644, 364
Baraffe I., Chabrier G., Allard F. & Hauschildt P.H. 1998, A&A 337, 403
Baraffe I., Chabrier G., Allard F. & Hauschildt P.H. 2002, A&A 382, 563
Baraffe I., Chabrier G., Barman T.S. et al. 2003, A&A 402, 701
Barrado Y Navascuès D., Stauffer J.R., Briceno C. et al. 2001, ApJS 134, 103
Barrado Y Navascuès D. & Jayawardhana R. 2004, ApJ 615, 840
Bessel M.S., PASP 102, 1181
Bessell M.S. 1991, AJ 101, 662
Bohlin R.C. & Gilliland R.L 2004, ApJ 128, 3053
Boulanger F., Bronfman L., Dame T.M. & Thaddeus P. 1998, A&A 332, 273
Briceño, Luhman K.L., Hartmann L. et al. 2002, ApJ 580, 317
Burgasser A.J. 2004,ApJ Supp. Ser. 155, 207
Burgasser A.J., Kirkpatrick J.D., McGovern M.R. et al. 2004, ApJ 604, 827
Burrows A. & Liebert J. 1993, Rev. of Modern Physics Vol. 65, No. 2, p. 301
Cambrésy L. 1999, A&A 345, 965
Cardelli J.A., Clayton G.C. & Mathis J.S. 1989, ApJ 345, 245
Chabrier G., Baraffe I., Allard F. & Hauschildt P. 2000, ApJ 542, 464
Chen H., Myers P.C., Ladd E.F. & Wood D.O.S. 1995, ApJ 445, 377
Chen H., Grenfell T.G., Myers P.C. & Hughes J.D. 1997, ApJ 478, 295
Chen B.C., Méndez, René A., Tsay W.S. & Lu P.K. 2001, ApJ 121, 309
Cieza, L. A., Kessler-Silacci, J. E., Jaffe, D.T., et al. 2005, ApJ, 635, 422
Cousins A.W.J. 1976, Mem. R. Astr. Soc. 81, 25
Covino E., Alcalá J. M., Allain S. et al. 1997, A&A 328, 187
Cutri R.M., Skrutskie M.F., Van Dyk S. et al. 2003, *Explanatory Supplement to the 2MASS All Sky Data Release*
Dahn C.C., Harris H.C., Vrba F.J. et al. 2002, AJ 124, 1170
D'Antona F. & Mazzitelli I. 1997, Mem. S.A.It. 68, 807
Ducati J.R., Bevilacqua C.M., Rembold S.B. & Ribeiro D. 2001, ApJ 558, 309
Dullemond C.P., Dominik C. & Natta A. 2001, ApJ 560, 957
Evans N.J. II, Allen L.E., Blake G.A. et al. 2003, PASP 115, 965
Feigelson E.D., Casanova S., Montmerle T. & Guibert J. 1993, ApJ 416, 623
Feigelson E.D. & Montmerle T. 1999, Ann. Rev. A&A 37, 363
Fernàndez M., Ortiz E., Eiroa C. & Miranda L.F. 1995, A&A Supp. Ser. 114, 439
Garay G., Mardones D., Rodrìguez L.F. et al. 2002, ApJ 567, 980
Giannini T., Mccoey C., Nisini B. et al. 2006, A&A, in press
Graham J.A. & Hartigan P. 1988, ApJ 95, 1197
Gray D.F. 1992, *The observations and analysis of stellar photospheres*, Cambridge Univ. Press
Gutièrrez Moreno A., Moreno H., Cortes G. & Wenderoth E. 1988, PASP 100, 973
Hamuy M., Walker A.R., Suntzeff N.B. et al. 1992, PASP 104, 533
Hartigan P. 1993 ApJ 105, 1511
Hauschildt P.H., Allard F. & Baron E. 1999, ApJ 512, 377
Henning T., Pfau W., Zinnecker H. & Prusti T. 1993, A&A 276, 129
Hillenbrand L.A. & Carpenter J. 2000, ApJ 540, 236
Hughes J.H. & Hartigan P. 1992, ApJ 104, 680
Jacoby G.H., Africano J.L. & Quigley R.J. 1987, PASP 99, 672
Jayawardhana R. & Ivanov V.D. 2006, in press
Jones T., Ashley M., Hyland A. & Ruelas-Mayoroga A. 1981, MNRAS 197, 413
Kenyon S.J. & Hartmann L. 1995, ApJ Supp. Ser. 101, 117
Kenyon S.J. & Hartmann L. 1995, ApJ Supp. Ser. 101, 117
Kroupa P. 2001, Mon. Not. R. Astron. Soc. 322, 231
Kroupa P. 2002, Science 295, 82
Kurucz R.L. 1979, ApJ Suppl. Ser. 40, 191
Landolt A.U. 1992, ApJ, 104, 340
Larson K.A., Whittet D.C.B., Prusti T. & Chiar J.E. 1998, A&A 337, 465
Lee H.T., Chen W.P., Zhi W.Z. & Jing Y.H. 2005, ApJ 624, 808
Leggett S.K., Allard F.,Berriman G. et al. 1996, ApJ Supp. Ser. 104, 117

López Martí B., Eislöffel J., Scholz A. & Mundt R. 2004, A&A 416, 555
López Martí B., Eislöffel J. & Mundt R. 2005, A&A 444, 175
Luhman K.L. & Rieke G.H. 1999, ApJ 525, 440
Luhman K.L. 1999, ApJ 525, 466
Luhman K.L., Rieke G.H., Young E.T. et al. 2000, ApJ 540, 1016
Luhman K.L., Stauffer J.R., Muench A.A. et al. 2003, ApJ 593,1093
Luhman K.L. 2004, ApJ 602, 816
Luhman K.L., D'Alessio P., Calvet N. et al. 2005, ApJ, 620, 51
Meyer M.R., Calvet N. & Hillenbrand L.A. 1997, ApJ 114, 288
Minezaki T. & Kobayashi Y. 1998, ApJ 494, 111
Monet D.G., Dahn C.C., Vrba F.J. et al. 1992, AJ 103, 638
Monet D., Bird A., Canzian B. et al. 1998, *The USNO-A2.0 catalogue*, U.S. Naval Observatory
Muench A.A., Lada E.A., Lada C.J. & Alves J. 2002, ApJ 573, 366
Muench A.A., Lada E.A., Lada C.J. et al. 2003, ApJ 125, 2029
O'Neal D., Neff J.E. & Saar S.H. 1998, ApJ 507, 919
Palla F. & Stahler S.W. 1999, ApJ 525, 772
Persi P., Marenzi A. R., Gómez M. & Olofsson G. 2003, A&A 399, 995
Porras A., Jorgensen, J.K, Allen, L. et al., 2006 submitted
Preibisch T., Stanke T. & Zinnecker H. 2003, A&A 409, 147
Preibisch T., McCaughrean M.J., Grosso N. et al. 2005, ApJ Supp. Ser. 160, 582
Prescott, M.K.M., Impey, C.D., Cool, R.J., Scoville, N. 2006, ApJ 644, 100
Prusti T., Whittet D.C.B., Assendorp R. & Wesselius P.R. 1992, A&A 260, 151
Reipurth B. & Clarck C. 2001, ApJ 122, 432
Schwartz R.D. 1977, ApJS 35,161
Schwartz R.D. 1991, ESO rep. No. 11, p. 93
Stetson P.B. 1987, PASP 99, 191
Stetson P.B. 2000, PASP 112, 925
Tinney C.G., Mould J.R. & Reid I.N. 1993, AJ 105, 1045
Vuong M.H., Cambrésy L. & Epchtein N. 2001, A&A 379, 208
White R.J.& Basri G. 2003, ApJ 582, 1109
Whittet D.C.B., Laureijs R.J., Zhang C.Y. 1991, A&A 251, 524
Whittet D.C.B., Prusti T., Franco G.A.P. et al. 1997, A&A 327, 1194
Young K.E., Harvey P.M., Brooke T.Y. et al. 2005, ApJ 628, 283
Zerbi F.M., Pallavicini R., Conconi P. et al. 2006, Mem. S.A.It. Suppl., Vol. 9, 419

Online Material

Table 7. Optical photometry of objects in the Cha II dark cloud. The positions for most objects are from the *R*-band images. For saturated objects in the *R*-band the positions are from the $H\alpha_{12}$ images; the coordinates of Sz 62, not observed in Hα, are from the *z*-band image. Magnitudes marked with an asterisk are taken from the the literature (see the relative references) and correspond to objects saturated in our images. Symbols and labels are as explained in the footnote. Comments about some of these objects are given in Appendix C.

Designation	RAJ2000 (hh:mm:ss)	DECJ2000 (dd:mm:ss)	R_c	I_c	z	$H\alpha_7$	$H\alpha_{12}$	m_{856}	m_{914}	Main Ref.	Note
IRAS 12416-7703	12:45:06.43	−77:20:13.52	S	S	S	11.86±0.09	12.10±0.13	S	S	i	•
IRAS 12448-7650	12:48:25.70	−77:06:36.72	S	S	S	13.15±0.09	13.55±0.13	S	S	i	•
IRAS F12488-7658	12:52:30.49	−77:15:12.92	14.84±0.01	12.21±0.02*	S	15.48±0.10	15.60±0.13	12.27±0.09	S	f,i	•
IRAS 12496-7650	12:53:17.17	−77:07:10.63	16.43±0.01	13.92±0.01	12.82±0.02	16.12±0.10	16.84±0.14	13.52±0.10	13.41±0.08	a	★
WFI J12533662-7706393	12:53:36.62	−77:06:39.31	22.22±0.14	19.35±0.04	18.00±0.04	ND	ND	19.26±0.20	18.58±0.12	m	NEW
C 17	12:53:38.84	−77:15:53.21	17.08±0.01	15.09±0.01	14.23±0.01	17.67±0.10	17.36±0.13	15.10±0.09	14.79±0.08	f	•
IRAS 12500-7658	12:53:42.79	−77:15:11.59	21.54±0.08	19.40±0.01	18.44±0.06	20.81±0.38	21.24±0.46	19.43±0.23	19.06±0.15	i	★ ✪
ChaII 304	12:55:16.00	−76:46:21.83	21.85±0.09	19.28±0.02	18.27±0.05	ND	ND	19.26±0.17	18.65±0.11	j	• ⌘
ChaII 305	12:55:16.48	−76:46:20.89	21.82±0.09	19.30±0.01	18.29±0.05	ND	ND	19.20±0.17	18.68±0.12	j	• ⌘
C 33	12:55:25.72	−77:00:46.62	16.86±0.01	15.16±0.01	14.66±0.01	17.15±0.22	16.93±0.13	15.22±0.09	14.79±0.08	f	•
2MASS12560549-7654106	12:56:05.43	−76:54:10.69	15.95±0.01	14.54±0.01	14.04±0.02	16.17±0.10	16.15±0.13	14.58±0.09	14.42±0.08	i	•
Sz 46NW	12:56:32.85	−76:45:44.78	18.45±0.01	17.69±0.17	17.56±0.04	18.72±0.13	18.70±0.14	17.96±0.10	18.07±0.09	a	• ⌘
Sz 46N	12:56:33.59	−76:45:45.18	14.61±0.01	13.16±0.01	12.68±0.01	14.80±0.10	15.07±0.13	13.24±0.09	13.08±0.08	a	★ ⌘
Sz 46S	12:56:33.64	−76:45:49.54	16.81±0.01	16.05±0.02	15.93±0.02	17.07±0.10	17.03±0.13	16.32±0.09	16.38±0.08	a	• ⌘
Sz 47	12:56:58.63	−76:47:06.72	13.86±0.01*	13.38±0.01*	13.45±0.01	13.68±0.10	14.07±0.13	13.72±0.09	13.86±0.08	a	★ ✰
IRAS 12533-7632	12:57:00.49	−76:48:35.10	21.19±0.12	19.76±0.01	ND	ND	20.90±0.38	19.92±0.33	19.83±0.29	e	•
IRAS 12535-7623	12:57:11.64	−76:40:11.14	13.61±0.01	12.13±0.01	11.53±0.02	13.69±0.10	13.73±0.13	12.22±0.09	12.03±0.08	e,i	•
ISO-CHA II 13	12:58:06.67	−77:09:09.22	22.51±0.27	19.38±0.01	17.89±0.04	ND	ND	19.44±0.19	18.33±0.11	g,k	★
WFI J12583675-7704065	12:58:36.75	−77:04:06.53	22.45±0.25	19.32±0.01	17.85±0.04	ND	ND	19.51±0.20	18.27±0.10	m	NEW
WFI J12585611-7630105	12:58:56.11	−76:30:10.48	16.39±0.01	14.38±0.01	13.54±0.02	16.08±0.09	16.60±0.13	14.34±0.09	13.81±0.08	m	NEW
C 41	12:59:09.86	−76:51:03.49	18.51±0.01	17.03±0.01	16.45±0.02	18.06±0.10	18.88±0.14	17.31±0.09	17.07±0.08	f,h	★ ✰
ISO-CHA II 29	12:59:10.19	−77:12:13.72	16.19±0.02	14.23±0.01	13.36±0.01	16.41±0.19	16.32±0.13	14.37±0.09	13.91±0.08	g,i	•
WFI J12591881-7704419	12:59:18.81	−77:04:41.92	15.69±0.01	14.09±0.01	13.34±0.01	15.86±0.10	15.88±0.17	14.19±0.09	13.86±0.09	m	NEW
WFI J12592348-7726589	12:59:23.48	−77:26:58.96	14.41±0.01	12.99±0.01	12.39±0.01	14.78±0.12	14.62±0.12	13.13±0.09	12.75±0.08	m	NEW
IRAS 12556-7731	12:59:26.50	−77:47:08.70	S	S	S	12.34±0.09	12.66±0.13	S	S	i	•
WFI J13005297-7709478	13:00:52.97	−77:09:47.77	22.63±0.30	19.64±0.07	18.25±0.05	ND	ND	19.85±0.25	18.66±0.12	m	NEW
Sz 48NE	13:00:53.15	−77:09:09.18	16.08±0.01	14.32±0.04	13.55±0.01	16.11±0.09	16.24±0.13	14.44±0.09	14.02±0.08	a	★ ⌘
Sz 49	13:00:53.26	−76:54:14.98	14.86±0.01	13.53±0.03	13.01±0.01	13.90±0.09	14.93±0.13	13.62±0.09	13.35±0.08	a	★ ✰
Sz 48SW	13:00:53.56	−77:09:08.28	16.26±0.01	14.50±0.02	13.72±0.01	16.13±0.09	16.57±0.13	14.51±0.09	14.19±0.08	a	★ ⌘
Sz 50	13:00:55.28	−77:10:22.01	14.42±0.01	12.50±0.01*	11.96±0.02	14.34±0.10	14.74±0.13	12.79±0.09	12.43±0.08	a	★
WFI J13005531-7708295	13:00:55.31	−77:08:29.54	14.93±0.01	13.29±0.01	12.64±0.01	15.26±0.14	15.24±0.13	13.39±0.09	13.15±0.09	m	NEW
RXJ1301.0-7654a	13:00:56.22	−76:54:01.76	11.59±0.01*	10.54±0.01*	10.17±0.01	11.63±0.09	11.71±0.14	10.61±0.09	10.66±0.09	d	★
IRAS F12571-7657	13:00:59.21	−77:14:02.80	18.62±0.01	16.16±0.01	15.00±0.01	19.26±0.14	19.23±0.16	16.48±0.23	15.79±0.14	e,g	•
ISO-CHA II 73	13:01:46.03	−77:16:02.89	16.31±0.02	15.12±0.01	14.68±0.01	16.71±0.22	16.55±0.13	15.38±0.09	15.13±0.08	g	•
WFI J13014752-7631023	13:01:47.52	−76:31:02.32	16.83±0.05	15.23±0.01	14.65±0.06	16.84±0.20	17.05±0.21	15.77±0.17	15.18±0.12	m	NEW
Sz 51	13:01:58.94	−77:51:21.74	13.47±0.02*	12.38±0.01*	11.80±0.02	12.46±0.09	13.37±0.13	12.55±0.09	12.29±0.08	a	★
CM Cha	13:02:13.49	−76:37:57.68	12.93±0.01	11.84±0.01	11.18±0.01	12.15±0.10	12.57±0.13	11.55±0.09	11.62±0.08	b	★
C 50	13:02:22.82	−77:34:49.51	17.78±0.01	15.49±0.02	14.53±0.01	17.78±0.10	18.19±0.20	15.48±0.09	14.93±0.08	f,g	•
IRAS 12589-7646	13:02:47.73	−77:02:46.32	S	S	S	12.72±0.09	12.92±0.13	S	S	i	•
RXJ1303.1-7706	13:03:04.46	−77:07:02.75	12.27±0.01*	11.17±0.01*	10.80±0.01	12.34±0.09	12.08±0.13	11.29±0.09	11.16±0.08	c	★
C 51	13:03:09.04	−77:55:59.52	16.88±0.01	14.47±0.01	13.46±0.02	16.82±0.10	17.16±0.13	14.39±0.09	14.03±0.10	f	•
ChaII 376	13:03:12.45	−76:50:50.82	16.31±0.01	15.45±0.01	15.35±0.05	16.40±0.10	16.42±0.13	NO	NO	j	•
WFI J13031615-7629381	13:03:16.15	−76:29:38.15	16.42±0.01	14.41±0.03	13.68±0.03	16.30±0.10	16.67±0.15	NO	NO	m	NEW
ISO-CHA II 98a	13:03:25.85	−77:01:48.36	17.09±0.02	16.42±0.04	16.24±0.03	17.53±0.10	17.27±0.11	16.83±0.09	17.17±0.24	g	• ⌘
ISO-CHA II 98b	13:03:26.10	−77:01:48.40	17.09±0.02	16.37±0.01	16.18±0.02	17.47±0.10	17.24±0.11	17.68±0.43	16.99±0.22	g	• ⌘
ISO-CHA II 110	13:04:18.96	−76:53:59.96	14.52±0.01	14.03±0.01	14.03±0.01	14.59±0.09	14.58±0.13	NO	NO	g	•

Table 7. Continued.

Designation	R.A.$_{J2000}$ (hh:mm:ss)	Dec.$_{J2000}$ (dd:mm:ss)	R_c	I_c	z	$H\alpha_7$	$H\alpha_{12}$	m_{856}	m_{914}	Main Ref.	Note
Hn 22	13:04:22.78	−76:50:05.86	13.51±0.01*	12.68±0.01*	12.17±0.02	13.23±0.09	13.85±0.13	NO	NO	b	★ ⌘
Hn 23	13:04:24.06	−76:50:01.39	12.23±0.01*	11.33±0.08*	S	12.11±0.09	12.34±0.13	NO	NO	b	★ ⌘ 👍
Sz 52	13:04:24.84	−77:52:30.11	16.89±0.01	14.94±0.01	14.12±0.01	17.00±0.10	17.35±0.13	14.84±0.09	14.43±0.08	a	★ 👍
Hn 24	13:04:55.74	−77:39:49.21	13.30±0.06*	11.95±0.02*	11.50±0.02	13.49±0.09	13.43±0.14	12.19±0.09	12.01±0.08	b	★ 👍
Hn 25	13:05:08.51	−77:33:42.66	16.11±0.01	14.17±0.02	13.36±0.01	16.45±0.12	16.61±0.13	14.40±0.09	14.01±0.09	b	★ 👍
Sz 53	13:05:12.66	−77:30:52.56	15.58±0.02	13.86±0.02	13.15±0.01	15.58±0.09	15.90±0.18	15.16±0.12	14.47±0.08	a	★ 👍
Sz 54	13:05:20.80	−77:39:01.48	11.58±0.02*	10.61±0.06*	10.47±0.43	11.28±0.10	11.57±0.13	10.80±0.09	11.05±0.15	a	★ 👍
Sz 55	13:06:30.49	−77:34:00.12	16.37±0.01	14.70±0.06	14.06±0.47	15.65±0.09	16.96±0.13	14.61±0.09	14.53±0.08	a	★ 👍
Sz 56	13:06:38.70	−77:30:35.39	15.41±0.01*	13.47±0.02*	12.71±0.44	15.41±0.09	15.75±0.13	13.67±0.09	13.15±0.08	a	★ 👍
Sz 57	13:06:56.56	−77:23:09.46	15.97±0.01	13.65±0.01	12.59±0.41	15.71±0.09	16.23±0.13	13.74±0.09	13.07±0.08	a	★ 👍
Sz 58	13:06:57.35	−77:23:41.46	14.63±0.01	13.16±0.01	12.53±0.43	14.44±0.09	14.58±0.13	12.98±0.09	12.78±0.08	a	★ 👍
Sz 59	13:07:09.23	−77:30:30.24	13.42±0.02*	12.08±0.01*	11.51±0.43	12.96±0.10	13.39±0.13	12.57±0.09	12.50±0.08	a	★ 👍
C 62	13:07:18.04	−77:40:53.00	18.60±0.01	16.10±0.01	15.00±0.44	18.42±0.11	18.97±0.17	16.23±0.09	15.60±0.08	f,l	• 👍
WFI J13071960-7655476	13:07:19.60	−76:55:47.64	18.33±0.01	16.49±0.02	15.77±0.02	18.12±0.10	18.57±0.14	NO	NO	m	👍 *NEW*
Sz 60W	13:07:22.30	−77:37:22.62	14.88±0.02*	13.45±0.02*	13.02±0.46	14.60±0.09	15.01±0.13	13.42±0.09	13.23±0.07	a	★ ⌘ 👍
Sz 60E	13:07:23.33	−77:37:23.20	15.32±0.02*	13.60±0.01*	12.94±0.46	15.01±0.09	15.69±0.13	13.98±0.09	13.61±0.08	a	★ ⌘
Hn 26	13:07:48.50	−77:41:21.73	16.07±0.01	14.31±0.01	13.54±0.46	15.89±0.11	16.25±0.13	14.41±0.09	14.13±0.08	b	★ 👍
Sz 61	13:08:06.33	−77:55:05.05	13.69±0.02*	12.38±0.01*	11.48±0.42	12.69±0.09	13.47±0.13	12.27±0.09	12.14±0.08	a	★ 👍
C 66	13:08:27.19	−77:43:23.41	18.91±0.01	16.51±0.01	15.44±0.44	19.24±0.14	19.72±0.22	16.76±0.09	16.03±0.08	f,l	• 👍
IRAS F13052-7653NW	13:09:09.81	−77:09:43.52	15.37±0.01	14.04±0.02	13.52±0.44	15.59±0.09	16.11±0.13	14.02±0.09	13.84±0.08	e	• ⌘
IRAS F13052-7653S	13:09:10.67	−77:09:46.84	13.49±0.01	12.57±0.01	12.38±0.47	13.09±0.09	13.04±0.13	12.69±0.09	12.77±0.08	e	• ⌘
IRAS F13052-7653N	13:09:10.98	−77:09:44.14	13.47±0.01	12.42±0.02	12.07±0.45	13.51±0.09	13.74±0.13	12.54±0.09	12.47±0.08	e	• ⌘
Sz 62	13:09:50.44	−77:57:23.94	14.03±0.02*	12.56±0.02*	11.66±0.43	NO	NO	NO	NO	a	★ 👍
Sz 63	13:10:04.12	−77:10:44.62	14.66±0.01	13.21±0.01	12.66±0.44	14.40±0.09	15.09±0.13	13.25±0.09	13.03±0.08	a	★ 👍
2MASS13102531-7729082	13:10:25.26	−77:29:08.70	16.49±0.01	15.36±0.05	14.95±0.48	16.49±0.10	16.49±0.13	15.54±0.09	15.43±0.08	i	• 👎
2MASS13110329-7653330	13:11:03.27	−76:53:32.89	14.50±0.01	13.85±0.00	13.68±0.01	14.62±0.09	14.57±0.13	NO	NO	i	• 👎
2MASS13125238-7739182	13:12:52.37	−77:39:18.58	15.36±0.01	13.62±0.02	12.97±0.47	15.57±0.09	15.78±0.13	13.83±0.09	13.51±0.08	i	• 👍
Sz 64	13:14:03.83	−77:53:07.48	15.82±0.01	14.01±0.01	13.16±0.45	15.25±0.09	16.29±0.13	14.40±0.09	13.65±0.08	a	★ 👍

Main references: a) Hughes & Hartigan (1992); b) Hartigan (1993); c) Alcalá et al. (1995); d) Covino et al. (1997); e)Alcalá et al. (2000); f) Vuong et al. (2001); g) Persi et al. (2003); h) Barrado y Navascuès & Jayawardhana (2004); i) Young et al. (2005); j) López Martí et al. (2005); k) Alcalá et al. (2006); l) Allers et al. (2006); m) This work.

Notes:

- ★ = Confirmed member
- • = Previously known candidate
- 👍 = Object recovered by our selection criteria
- 👍 *NEW* = Member candidate firstly identified in this work
- 👎 = Object rejected on the basis of our selection criteria
- ✯ = Veiled object
- ✪ = Embedded object
- ⌘ = Component of a visual binary or multiple system
- S = Saturated object
- ND = Object not detected
- NO = Object not observed

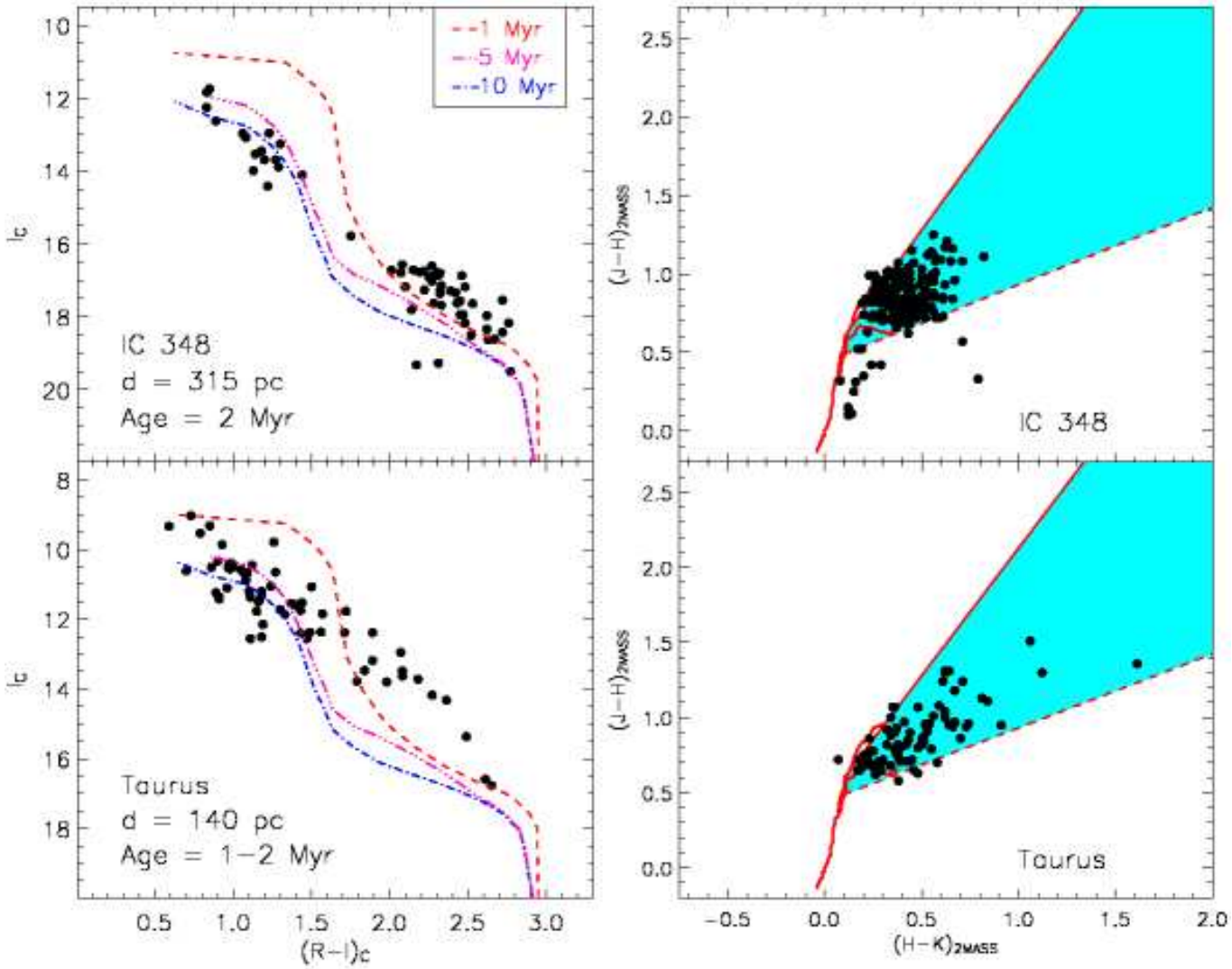

Fig. 14. I_C vs. $(R-I)_C$ and $(J-H)$ vs. $(H-K)$ diagrams for the PMS populations in Taurus and IC348. The isochrones, shifted by the corresponding distance modulus, are as in Fig. 9. The selection limits in the $(J-H)$ vs. $(H-K)$ diagrams are as in Fig. 10.

Appendix A: Flux at $z = 0$

In order to derive the flux at zero magnitude in the z band we used the following procedure:

1. The spectrophotometry of SA 98 653 is available from Gutièrrez Moreno et al. (1988) in the form of monochromatic instrumental magnitudes, covering a wavelength range from 3200 to 8000 Å, in steps of 40 Å for $\lambda \leq 5400$ Å and 80 Å for $\lambda > 5400$Å. Since the z band is centered at 9648 Å (FWHM=616 Å), we need the spectrophotometry in a wider wavelength range. We have thus extrapolated the SED of SA 98 653, up to 16000 Å, by using the Kurucz grid of stellar atmosphere models (Kurucz 1979) in the following way. We first dereddened the SED of SA 98 653 using the canonical absorption-to-reddening ratio R_V=3.2, as suggested by Chen et al. (2001) for the SA 98 field. Assuming that SA 98 653 is a main sequence star, as indicated by its spectrophotometry and broad-band photometric indexes, we derived its distance by comparing its observed V magnitude with the expected absolute visual magnitude ($M_V = 0.7$, Gray 1992) for an A0-type main sequence star. Assuming an error of two spectral sub-classes on SA 98 653 spectral type, we constrained its distance between 300 and 450 pc, i.e. 0.30 mag< A_V <0.45 mag. Note that the extinction of the nearby star SA 98-667 (spectral type B9V) is A_V=0.33 calculated from its Hipparcos parallax (Chen et al. 2001), which is consistent with the range of values allowed for SA 98 653. The interstellar extinction coefficients at each wavelength were derived by using the extinction curve by Cardelli et al. (1989). We then performed a two-parameters least-square fit to the observed spectrophotometry of SA 98 653 by taking as free parameters the extinction (in the range 0.30 mag< A_V <0.45 mag in steps of 0.01 mag) and the effective temperature of the model spectrum. Both the Kurucz models and the dereddened SED of SA 98 653 were normalised to the flux at 5556 Å. A minimum χ^2 for a model with $T_{\rm eff}$ = 11000 K, $\log g$=4 and A_V=0.33 was derived (Fig. A.1). We then used this synthetic spectrum reddened with A_V=0.33 to extrapolate the spectrophotometry of SA 98 653 in the near-IR.
2. The absolute Earth flux at 5556 Å of a star with magnitude V^* calibrated with Vega, the primary photometric standard, is given by (Gray 1992):

$$log(F^*_{5556}) = -0.400 \cdot V^* - 8.451 \qquad (A.1)$$

in units of erg $\cdot$ cm^{-2} $\cdot$ s^{-1} $\cdot$ Å^{-1}.
When this expression is used for stars whose effective temperature is different from Vega ($T_{\rm eff}$ = 9790 K), as in the case of SA 98 653, a small systematic error is introduced because the effective wavelength of the V band is 5480 Å, i.e. 76 Å shorter than the reference wavelength (5556 Å). An adequate correction for this is given by the following colour term (Gray 1992):

$$log\left(\frac{F^*_{5556}}{F^*_{5480}}\right) = -0.006 + 0.018 \cdot (B-V)^* \qquad (A.2)$$

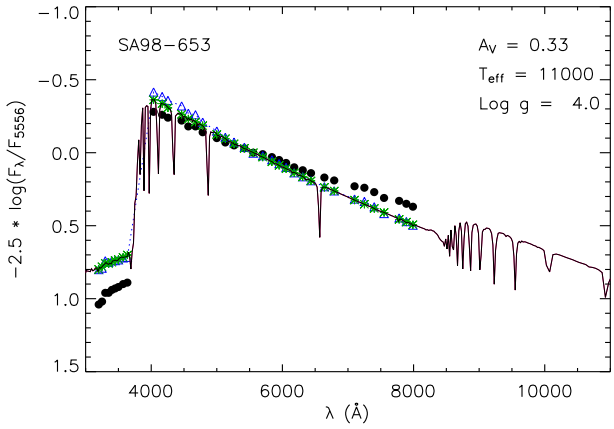

Fig. A.1. Observed (dots) and dereddened (open triangles) spectral energy distribution of SA 98 653 normalised to the flux at 5556 Å. The best fitting model by Kurucz (1979) is overplotted (continuous line).

Considering the dereddened visual magnitude of SA 98 653 and its intrinsic $(B-V)$, and applying Eq. A.2 and Eq. A.1 respectively, we obtain:

$$V^{corr}_{SA\ 98\ 653} = 9.24$$

and

$$log[F^{5556}_{SA\ 98\ 653}] = -12.1465$$

We now can calculate the flux of SA 98 653 at any wavelength with respect to the flux at 5556 Å as:

$$F^{synt}_{SA\ 98\ 653}(\lambda) = F^{5556}_{SA\ 98\ 653} \cdot 10^{-0.4 \cdot mag^{synt}_{SA\ 98\ 653}(\lambda)} \qquad (A.3)$$

where $mag^{synt}_{SA\ 98\ 653}$ is the synthetic magnitude of SA 98 653 at each wavelength normalised to the magnitude at 5556 Å, determined in the previous step.

3. We finally determined the synthetic flux of SA 98 653 in the z band by integrating its synthetic spectrum $F^{synt}_{SA\ 98\ 653}(\lambda)$ in the z filter transmission curve T_λ, i.e. the product of the detector quantum efficiency and the filter transmission curve:

$$F^z_{SA\ 98\ 653} = \frac{1}{A_z} \cdot \int_{\lambda_1}^{\lambda_2} F^{synt}_{SA\ 98\ 653}(\lambda) \cdot T_\lambda \cdot d\lambda \qquad (A.4)$$

where:

$$A_z = \int_{\lambda_1}^{\lambda_2} T_\lambda \cdot d\lambda \qquad (A.5)$$

We obtained:

$$F^z_{SA\ 98\ 653} = 1.62 \cdot 10^{-13} \quad erg \cdot cm^{-2} \cdot s^{-1} \cdot Å^{-1}$$

$F^z_{SA\ 98\ 653}$ is the flux in the z filter of an A0 type star with visual magnitude V = 9.539 and $z = I_C$ = 9.522. What we need, in order to obtain an absolute flux calibration for the

z band, is the flux of an A0-type star with $V = 0$ and $z = 0$ (F^z_{A0V}). Since SA 98 653 is an A0-type star and we have defined its intrinsic colour as $(I_C - z) = 0$, we have:

$$z_{SA\ 98\ 653} \stackrel{\text{def}}{=} I_{SA\ 98\ 653} = 9.522 \quad \text{(A.6)}$$

Thus, we derive F^z_{A0V} as:

$$F^z_{A0V} = F^z_{SA\ 98\ 653} \cdot 10^{(0.4 \cdot z_{SA\ 98\ 653})} \quad \text{(A.7)}$$

By considering the uncertainties on magnitude and interstellar extinction measurements, we obtained:

$$F^z_{A0V} = (8.4 \pm 0.1) \cdot 10^{-10} \ \text{erg cm}^{-2}\text{s}^{-1}\text{Å}^{-1}$$
$$= (2608 \pm 31)\ \text{Jy}$$

A slightly smaller absolute flux calibration constant for the WFI z band has been estimated by F. Coméron (private communication) using the absolute flux calibration of Vega obtained by Bohlin & Gilliland (2004) with the Space Telescope Imaging Spectrograph (STIS). Using these data we derive a value of $7.2 \cdot 10^{-10}$ erg $\cdot$ cm^{-2} $\cdot$ s^{-1} $\cdot$ Å^{-1}. However, for the sake of homogeneity, we prefer to use the value we derive above.

Appendix B: Isochrones

In order to transform the colours and magnitudes of the isochrones reported by Baraffe et al. (1998) and Chabrier et al. (2000) into the WFI-Cousins system we determined first the WFI synthetic magnitudes, $m_{\Delta\lambda}$:

$$m_{\Delta\lambda} = -2.5 \cdot log_{10}(f_{\Delta\lambda}) + C_{\Delta\lambda} \quad \text{(B.1)}$$

where $C_{\Delta\lambda}$ is the absolute calibration constant of the photometric system, tied to the Earth flux of an A0-type star with magnitude $V = 0$ (see Tab. 5), and $f_{\Delta\lambda}$ is the observed flux.

In order to compute the expected flux of a PMS star or a young BD in the pass-band $\Delta\lambda$ of a given filter we proceeded as follows. We first determined the transmission curve, T_λ, i.e. the product of the detector quantum efficiency and the given filter transmission curve[7]. We then computed:

$$f_{\Delta\lambda} = \frac{1}{A_{\Delta\lambda}} \cdot \int_{\lambda_1}^{\lambda_2} F_\lambda \cdot T_\lambda \cdot d\lambda \quad \text{(B.2)}$$

where

$$A_{\Delta\lambda} = \int_{\lambda_1}^{\lambda_2} T_\lambda \cdot d\lambda \quad \text{(B.3)}$$

and F_λ is the absolute flux of a given PMS star or BD. For this purpose we used the synthetic low-resolution spectra for low-mass stars by Hauschildt et al. (1999) calculated with their NextGen model-atmosphere code. For simulating very cool objects (i.e. $T_{\rm eff}$ <3000 K) we used the StarDusty and BD-Dusty atmosphere models by Allard et al. (2000), which include dust opacity.

[7] Available at: http://www.ls.eso.org/lasilla/sciops/2p2/E2p2M/WFI/filters.

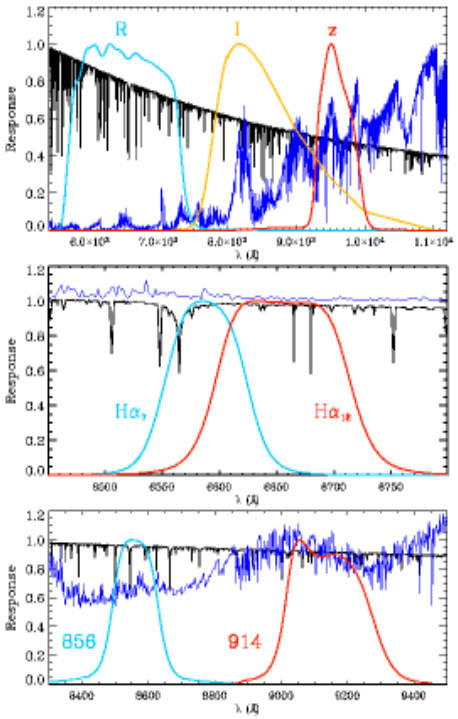

Fig. B.1. The R, I, z (upper panel), $H\alpha_7$, $H\alpha_{12}$ (central panel), 856 and 914 nm (lower panel) WFI+ESO2.2m transmission bands. Examples of two normalised NextGen spectra (Hauschildt et al. 1999) with $T_{\rm eff}$=2500 K and $T_{\rm eff}$=6000 K are over-plotted.

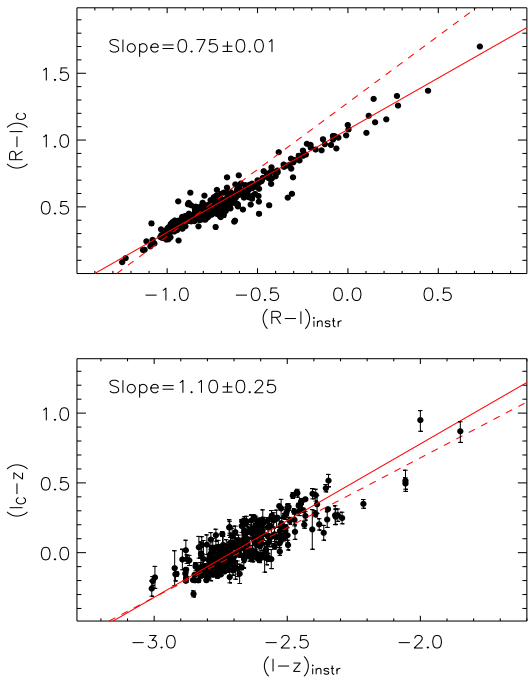

Fig. B.2. The Cousins colours as a function of the WFI instrumental colours for the standard stars in the Landolt's field SA 98. The continuous lines display the best fit of the data while the dashed lines have slope equal to 1 (i.e. no correction).

As an example of our procedure we show in Fig. B.1 (upper panel) two model spectra and the *R*, *I* and *z* WFI+ESO2.2m transmission curves over-plotted. However, the flux $f_{\Delta\lambda}$ that we obtained in this way is the one at the surface of the star. The observed flux at any distance (d) is given by:

$$f_{\Delta\lambda}(d) = f_{\Delta\lambda} \cdot \left(\frac{R^{\star}}{d}\right)^2 \quad \text{(B.4)}$$

where R* is the object radius. The values for R* can be computed from theoretical PMS evolutionary tracks, which in our case are those by Baraffe et al. (1998) for low-mass stars and those by Chabrier et al. (2000) for sub-stellar objects (i.e. M$\lesssim 0.1 M_{\odot}$). Finally, setting d=10 pc and using Eq. B.1, one can derive the absolute magnitudes for a given T$_{\rm eff}$, age and R* and hence, determine the isochrones in the CMDs.

Note that, consistently with the *RIz* photometric calibration of the sources in Cha II, the absolute calibration constants used in Eq. B.1 are those of the WFI-Cousins photometric system (see Tab. 5). However, a non-negligible difference between the *I*-WFI and the *I*-Cousins pass-bands arises from the fact that the red cut-off of the *I*-WFI filter is defined by the CCD response and it is centered at a redder wavelength (0.85μm) with respect to the standard Cousins *I* filter (0.79μm). In order to take into account this difference in the determination of the theoretical isochrones, we have exploited the relations between the WFI-Cousins $(R-I)_C$ and $(I_C - z)$ standard colours and the WFI instrumental colours for the standard stars in the Landolt's fields. By a least-square linear fitting (Fig. B.2), we derive the coefficients which allow us to correct the colours of the computed isochrones:

$$(R-I)_{synt} = 0.75 \cdot (R-I)_{instr} \quad \text{(B.5)}$$

$$(I-z)_{synt} = 1.10 \cdot (I-z)_{instr} \quad \text{(B.6)}$$

In this way we were able to report in the WFI-Cousins photometric system the isochrones originally calculated by Baraffe et al. (1998) and Chabrier et al. (2000) in the Cousins system of Bessel (Bessel 1990). This allows us to use the isochrones in a photometrically homogeneous way.

In Fig. B.3 the 1, 5 and 10 Myr isochrones by Chabrier et al. (2000) are compared with those derived by us in the WFI-Cousins photometric system. Note the large difference, in particular for the coolest objects, i.e. $(R-I)_C$ >1.7, where the use of the isochrones in the Bessel-Cousins system would have produced many spurious member candidates.

In order to check our procedure, we used the standard filters of Bessel (1990) and we were successful in reproducing the isochrones presented by Chabrier et al. (2000) (see the smaller panel in Fig. B.3).

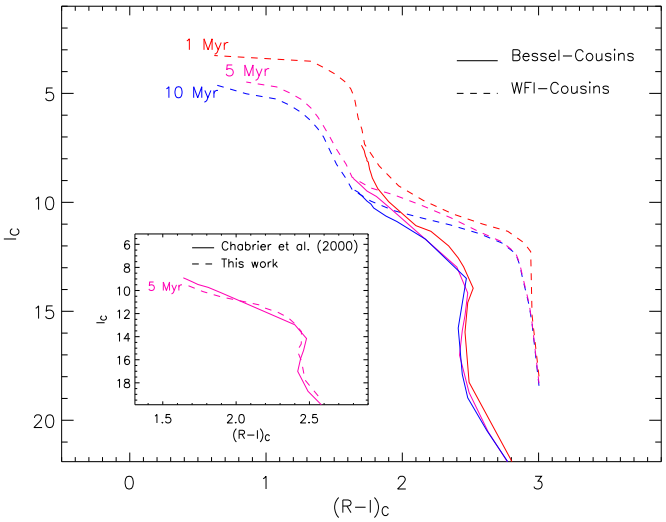

Fig. B.3. Theoretical isochrones by Baraffe et al. (1998) and Chabrier et al. (2000) for the Cousins photometric system of Bessel (continuous line) and for the WFI-Cousins system (dashed lines, this work). In the smaller panel the 5 Myr isochrone by Chabrier et al. (2000) (continuous line) is compared with that reproduced by our algorithm when using the same Bessel filters (dashed line).

Appendix C: Comments on individual objects

IRAS 12416-7703, IRAS 12448-7650, IRAS F12488-7658, IRAS 12556-7731, IRAS 12589-7646

These objects were selected as member candidates of Cha II by Young et al. (2005) on the basis of MIPS@Spitzer observations. IRAS F12488-7658/C 13 was also previously proposed as a young object by (Vuong et al. 2001). We cannot conclude whether our selection criteria are satisfied for these objects because they are saturated in at least one of the three broad-bands *RIz*. However, their $(H\alpha_{12} - H\alpha_7)$ indices suggest Hα emission (see Tab. 7) at $\sim 2\sigma$ level and their location on the $(J-H)$ vs. $(H-K)$ diagram is consistent with the PMS stars locus (see Sec. 4 and Fig. 10).

ChaII 304, ChaII 305, ChaII 376

ChaII 376 was the only Hα emitter detected by López Martí et al. (2005) in their WFI pointing. They also proposed that their candidates ChaII 304 and ChaII 305 are two low-mass BDs or planetary-mass objects close to the Deuterium burning limit. These two objects, however, do not satisfy our selection criteria. The early classification of these objects as possible Cha II members by López Martí et al. (2005), though based on WFI images taken with the same set of filters as in our survey, is probably not accurate because the isochrones in the Cousins system of Bessel (Chabrier et al. 2000) used for the selection are inadequate for the WFI-Cousins photometric system (see Appendix B). From their dereddened $(m_{856} - m_{914})$ colour index we estimate an effective temperature of 2800 K and 3000 K for ChaII 304 and ChaII 305, respectively. Assuming these temperature values, we find that the location of the two objects on the HR diagram would be inconsistent with membership to Cha II. We found that the optical colours of ChaII 376 are inconsistent with membership, as also asserted by López Martí et al. (2005), and we do not detect any significant Hα emission for this object. Moreover, its *R*-band magnitude (16.31 mag) is remarkably

brighter than the one reported by López Martí et al. (2005) (18.38 mag). Since the magnitude of this object in the other bands are in fair agreement with ours, we think that the *R*-band magnitude reported in López Martí et al. (2005) may be incorrect. This may explain why ChaII 376 was selected as their only Hα emitter.

Sz 46

This is one of the 19 PMS stars originally identified by Schwartz (1977) in Cha II. Subsequent photometric observations by Hughes & Hartigan (1992) showed that the object is a visual triple system. The Hα emission star originally discovered by Schwartz (1977), Sz 46N, has two companions, namely Sz 46NW and Sz 46S; both are bluer than Sz 46N and are probably unrelated to it (Hughes & Hartigan 1992). Based on our analysis, both Sz 46NW and Sz 46S have optical colours inconsistent with membership to the Cha II cloud, their temperature is well above 4000 K according to their ($m_{856} - m_{914}$) index and the ($H\alpha_{12} - H\alpha_7$) colour suggests no Hα emission. Thus, Sz 46NW and Sz 46S are most probably not PMS stars and hence, not physically associated with Sz 46N.

IRAS 12533-7632, IRAS F13052-7653

These objects were detected as ROSAT X-rays sources (Alcalá et al. 2000) and proposed as possible members of Cha II by different authors (Larson et al. 1998; Prusti et al. 1992; Young et al. 2005).

IRAS 12533-7632 appears on our images as a point-like object associated with a nebulosity, consistently with what reported in Prusti et al. (1992). However, it was not detected in our *z* and Hα images; its *RI* magnitudes and 2MASS near-IR colours are inconsistent with those expected for a PMS star.

In Young et al. (2005) IRAS F13052-7653 is reported as CHIIXR 60 which is a non-existent identifier. This must be a typo because IRAS F13052-7653 is identified with the ROSAT source CHIIXR 37 (Alcalá et al. 2000). The optical counterpart of IRAS F13052-7653 appears as a visual triple system (Larson et al. 1998) whose components are designated as IRAS F13052-7653N, IRAS F13052-7653NW and IRAS F13052-7653S in Tab. 7. None of the three components was recovered by our selection criteria, most likely because their colours, both in optical and and near-IR, may be contaminated. However, two of them, namely IRAS F13052-7653N and IRAS F13052-7653NW, fall just below the 10 Myr isochrone and their ($H\alpha_{12} - H\alpha_7$) indices suggest Hα emission above 3σ level (see Tab. 7); moreover, their near-IR colours are also consistent with those expected for PMS stars. IRAS F13052-7653S is not detected in 2MASS; its optical colours are inconsistent with membership to Cha II and its Hα colour does not indicate significant emission.

IRAS F12571-7657

This object was detected in X-rays with ROSAT (Alcalá et al. 2000). Its optical and near IR colours are consistent with those of a PMS star with strong IR excess (see also Young et al. 2005). Previous authors (Allers et al. 2006; Vuong et al. 2001) report an extinction value significantly higher than what we determine from the Cambrésy (1999) extinction map. Given the strong IR excess, our procedure for the temperature estimate provides unreliable results. Therefore, it may be a deeply embedded source or a highly reddened PMS star.

C 62, C 66

These sources have been firstly detected by DENIS and proposed as young stellar object candidates of Cha II by Vuong et al. (2001) based on their IR colours and, more recently, by Young et al. (2005) and Allers et al. (2006) on the basis of IRAC@Spitzer and MIPS@Spitzer observations respectively. From the effective temperature and A_V estimates provided in Tab. 6, and calculating their luminosities as explained in Sec. 5, we estimate a mass of 0.08 and 0.06 $M_\odot$ for C 62 and C 66, respectively. The age we derive for both objects using the Baraffe et al. (1998) tracks is around 2 Myr. These estimates of mass and age are fairly consistent with those derived by Allers et al. (2006). From their Hα index we also notice strong line emission ($\sim$3σ level) in both objects (see Tab. 6).

ISO-CHA II 29

This source has been detected in the near and mid-IR by Persi et al. (2003), but it was first revealed as an X-ray emitting source, CHIIXR3, by Alcalá et al. (2000). The association of this object with IRAS 12551-7657 is still unclear. Based on these evidences and the effective temperature estimated by us (Tab. 6), ISO-CHA II 29 is proposed to be a PMS star in Cha II with a mass of about 1 $M_\odot$.

ISO-CHA II 73, ISO-CHA II 98, ISO-CHA II 110

None of these sources, originally identified by Persi et al. (2003), were selected with MIPS@Spitzer by Young et al. (2005). These sources do not satisfy our criteria and their ($H\alpha_{12} - H\alpha_7$) index suggests no emission in Hα.

In our optical images ISO-CHA II 98 appears as a visual binary, but the colours and magnitudes of its components are inconsistent with our selection criteria. We stress that ISO-CHA II 98 has been wrongly identified in SIMBAD with the ROSAT X-ray source CHIIXR 24 by Alcalá et al. (2000). The optical spectrum of CHIIXR 24 shows the Li I 6708Å absorption line, but the Hα line is well in absorption (Alcalá et al. 2000). Being classified as a G7-type star, CHIIXR 24 is most likely a field object unrelated to Cha II.

2MASS 13102531-7729085, 2MASS 13110329-7653330, 2MASS 13125238-7739182

These sources are reported in the list of candidates by Young et al. (2005). While 2MASS 13102531-7729085 and 2MASS 13110329-7653330 are rejected by our selection crite-

ria, 2MASS 13125238-7739182 is selected as a PMS star candidate. The former two sources have Hα indices indicating no Hα emission, while the Hα index of the latter suggests Hα in emission at 1σ level. Thus, it is likely that 2MASS 13102531-7729085 and 2MASS 13110329-7653330 are field stars unrelated to Cha II.